# Aerosol UV absorption experiment (2002-04): 2. Absorption optical thickness and single scattering albedo

N.A. Krotkov[*a], P.K. Bhartia[b] and J.R.Herman[b], Jim Slusser[d],

Gwen Scott[d], G. Labow[c], A. Vasilkov[c], T. F. Eck[a], O. Dubovik[a], and B. N. Holben[b]

[a]Goddard Earth Sciences and Technology Center Univ. of Maryland Baltimore County, MD USA;

[b]NASA Goddard Space Flight Center, Greenbelt, MD USA;

[c]Science Systems and Applications, Inc., Lanham, MD USA 20706

[d]USDA UVB Monitoring Network and Colorado State University

[*] Krotkov@chescat.gsfc.nasa.gov; phone 1 301 614-5553; fax 1 301 614-5903; http://toms.gsfc.nasa.gov; GEST Center, NASA/GSFC Code 916 Greenbelt, Maryland 20771

## ABSTRACT

Compared to the visible spectral region very little is known about aerosol absorption in UV. Without such information it is impossible to quantify the causes of the observed discrepancy between modeled and measured UV irradiances and photolysis rates. We report results of an aerosol UV absorption closure experiment where a UV-shadow-band radiometer (UV-MFRSR, USDA UVB Monitoring and Research Network) and well-calibrated sun-sky radiometer (CIMEL, NASA AERONET network) were run side-by-side continuously for 17 months at NASA/GSFC site in Greenbelt, MD. The aerosol extinction optical thickness, $\tau_{ext}$, was measured by the CIMEL direct-sun technique in the visible and at two UV wavelengths 340 and 380 nm. These results were used for UV-MFRSR daily on-site calibration and measurements of $\tau_{ext}$ at 368nm . The $\tau_{ext}(368)$ measurements were used as input to a radiative transfer model along with AERONET retrievals of the column-integrated particle size distribution (PSD) to infer an effective imaginary part of the UV aerosol refractive index, k. This was done by fitting MFRSR measured voltage ratios with the radiative transfer model. Inferred values $k_{368}$ allow calculation of the single scattering albedo, $\omega_{368}$, and comparisons with AERONET $w_{440}$ retrievals. Using all cases for cloud-free days, we derive diurnal and seasonal dependence of the aerosol absorption optical thickness, $t_{abs}$ at 368nm with an uncertainty 0.01–0.02 limited by the accuracy of total voltage ($V_T$) measurement and calibration ($V_0$). The variability in aerosol size distribution and real refractive index becomes comparable to the measurement uncertainties only for large aerosol loadings ($t_{ext}$>0.5). The $t_{abs}$ follows pronounced seasonal dependence with maximum values ~0.07 occurring in summer hazy conditions and <0.02 in winter-fall seasons, when aerosol loadings are small. We also found that $\omega$ decreases with decrease in extinction optical thickness, suggesting different aerosol composition in summer and winter months.


**Keywords:** ultraviolet radiation, aerosol absorption, single scattering albedo, CIMEL sun photometer, AERONET network, UV multi-filter rotating shadow band radiometer, UV MFRSR, diffuse fraction measurements

## 1. INTRODUCTION

Absorption by black carbon and other absorbing aerosol components (mineral dust, nitrated and aromatic aerosols and organics) in the UV is of interest to tropospheric chemistry because it changes the rate of photochemical reactions and smog production[1-3] as well as penetration of biologically harmful UV radiation to the surface[4-13]. However, absorption properties of aerosols in the UV are poorly known, which makes it difficult to quantify a cause for the observed discrepancy in UV irradiances and photolysis rates estimated from satellite data and those measured at the ground[11,14].

The goal of this paper is to quantify the UV aerosol absorption required to bring model calculations of diffuse atmospheric transmittance with measurements from UV-shadow-band radiometer (UV-MFRSR, USDA UVB Monitoring and Research Network)[15-17] into agreement, while other model input parameters are constrained using independent co-located measurements. The ancillary measurements include sun-sky radiometer (CIMEL Electroninique CE-318) aerosol data from the

AERONET global network[18,19] (available from http://aeronet.gsfc.nasa.gov ), total ozone measured by a double Brewer spectrometer, and surface pressure measurements. Direct sun CIMEL measurements of spectral aerosol extinction optical thickness, $t_{ext}$, were used for UV-MFRSR on-site calibration (daily $V_0$ estimates) to ensure accurate measurements of UV-MFRSR $t_{ext}$ ($\sigma_{\Delta\tau} < 0.02$), as described in the first part of the paper. In addition, AERONET almucantar inversions of column-integrated particle size distribution (PSD) and effective refractive index[25,26] at visible wavelengths were used to constrain model input and compare aerosol absorption retrievals between UV and visible wavelengths. Essentially, we performed first aerosol column absorption closure experiment in UV, in which apparent effects of aerosol absorption could be separated from effects caused by variability in aerosol size distribution or gaseous absorption by ozone.

Section 2 describes the data sets used in this study in more detail. This is followed by an accuracy assessment of MFRSR aerosol UV absorption retrievals (section 3). Section 4 provides description of the MFRSR inversion implementation and section 5 discusses results and comparisons with AERONET aerosol single scattering albedo data at 440nm. Section 6 provides daily statistics of UV aerosol absorption optical thickness for 17 months of continuous MFRSR operation at NASA GSFC site and section 7 discusses implications for surface UV estimates from satellite instruments (TOMS, GOME, OMI).

## 2. DATA SETS

The UV-MFRSR is a shadow-band instrument that measures voltages proportional to diffuse and total horizontal irradiance[16,17]. A single measurement cycle consists of measuring total horizontal irradiance (no sun blocking) following by 3 irradiance measurements with different positions of the shadow band blocking the sun and aureole on each side of the sun (Figure 1). The complete cycle takes ~10sec and is repeated every 3min throughout the day. All spectral channels are measured simultaneously by 7 separate solid-state detectors that share a common diffuser[16]. MFRSR instrument was installed at the AERONET primary calibration site at NASA Goddard Space Flight Center (GSFC) in Maryland with routine operation started on October 1, 2002. The instrument's location is on an elevated rooftop platform that allows an unobstructed view of the horizon. The raw data (voltages) were automatically transmitted to the USDA-UVB network processing center for calibration and further processing. The instrument's operation was remotely monitored and controlled by USDA-UVB network processing center at Colorado State University at Fort Collins, Co. The standard USDA-UVB network data processing includes calculation of cosine corrected diffuse horizontal, direct-sun normal and total components of the irradiance using CUCF measured spectral and angular response functions and applying absolute radiometric (lamp) calibration to all irradiance components. The 3-min standard data were aggregated in monthly files (available on the UVB program web site http://uvb.nrel.colostate.edu/UVB/home_page.html). For aerosol absorption retrievals we only use cosine corrected voltage ratios, as described later.

Co-located CIMEL Electroninique CE-318 Sun-sky radiometer measurements were made with reference instruments of the AERONET global network[18,19]. The automatic tracking Sun and sky scanning radiometers made direct sun measurements with a $1.2^o$ full field of view every 15 minute at 340, 380, 440, 500, 675, 870, 940 and 1020nm. The CIMEL $t_{ext}$ measurements (accuracy

typically ~0.003 to 0.01 in the visible with higher errors in the UV[29]) were interpolated in time and wavelength to match MFRSR 3-min measurements as described in the first part of the paper. Cloud-screened[30] CIMEL sky radiance almucantar measurements at 440nm, 675nm, 870nm and 1020nm were used in conjunction with the direct-sun measured aerosol $t_{ext}$ at these wavelengths to retrieve column average aerosol size distribution (PSD) and effective refractive index (real and imaginary part independently at each wavelength) following the methodology of Dubovik and King[25]. The inversion allows estimation of spectral single scattering albedo, ω, between 440 and 1020nm with an uncertainty of ~0.03 depending on aerosol type and optical depth [26,27].

Ancillary measurements at our site include total ozone measurements by a Brewer double spectrophotometer and pressure measurements. Cloud–free periods without snow were manually selected from the dataset. Low surface albedo in UV ~0.02 at GSFC site was confirmed from satellite overpass reflectivity measurements from Earth Probe Total Ozone Mapping Spectrometer (TOMS) on clear snow-free days. Such low values of surface albedo provide an important advantage for measuring aerosol properties in UV spectral range.

## 3. SENSITIVITY OF UV-MFRSR MEASUREMENTS TO AEROSOL ABSORPTION

Standard MFRSR measurements include voltages that are proportional to total horizontal and diffuse horizontal irradiance components. Since both components are measured by the same diffuser/filter/detector combination, diffuse and total atmospheric transmittances are obtained directly from the voltage ratios: $T_D = V_D/V_0$ and $T_T = V_T/V_0$. Here $V_0$ is extraterrestrial voltage obtained by calibration transfer from AERONET network sun-photometers[18,19] as explained in the first part of the paper. The diffuse and total transmittances are not independent, since voltage difference ($V_T$ - $V_D$) has been used for calibration (to determine $V_o$) and to infer aerosol extinction optical thickness, $t_{ext}$,. Therefore, only one additional aerosol parameter could be inferred independently in each MFRSR spectral channel by fitting either transmittance (or their ratio) to a radiative transfer model. Our goal is to infer aerosol absorption optical thickness, $t_{abs}$, while other model input parameters are constrained by independent measurements. We note that UV surface albedo is low and stable at our site for snow free conditions (~0.02-0.03 from clear-sky overpass EP/TOMS reflectivity measurements), and thus, does not have a noticeable effect on ground based aerosol measurements.

Historically, different irradiance ratios were used to infer $t_{abs}$ (or aerosol single scattering albedo, $\omega=1-\tau_{abs}/\tau_{ext}$): diffuse/direct ratio, $DD=T_D/(T_T-T_D)$[13, 20-22], diffuse fraction (diffuse/total, $DT=T_D/T_T$) ratio[23,24] and total to Rayleigh transmittance ratio ($TR=T_T/T_{Ray}$ )[6]. In the end, all inversion techniques should deliver consistent $t_{abs}$ retrieval results regardless of which input data are used. However, it turns out that for the estimation of $t_{abs}$ the most convenient quantity is the total ($T_T$ =*direct plus diffuse*) atmospheric transmittance, which is directly related to aerosol absorption and is least sensitive to aerosol size distribution and extinction optical thickness, $t_{ext.}$ In the UV spectral region, where $t_{\text{Rayleigh}}$ typically exceeds that of $t_{\text{aerosol}}$, it is convenient to normalize $T_T$ by total transmittance of molecular atmosphere with the same ozone amount, $TR=T_T/T_{Ray}$, which greatly

reduces sensitivity to ozone, wavelength and solar zenith angle. An important advantage of working with TR is that non-absorbing aerosols have only a small effect on *TR* (τ~0.1 produces ~1% *TR* reduction)[6], since the decrease in direct solar flux caused by aerosol scattering is nearly compensated by an increase in diffuse sky flux. For UV absorbing aerosols (*dust*, *smoke* and *urban*) the increase in the diffuse flux is suppressed by aerosol absorption, so *TR* sensitivity to $t_{abs}$ is an order of magnitude greater than *TR* sensitivity to $t_{ext}$ . Based on modeling study[6] the dependence of *TR* on $t_{ext}$ and $t_{abs}$ can be written approximately as:

$$-\ln(TR) \approx a t_{ext} + b t_{abs} \qquad (1)$$

where, for typical aerosols (not containing significant quantities of mineral dust and smoke), a~0.1 and b~2-3 (increasing with solar zenith angle). To better estimate a and b we use aerosol properties measured at GSFC. We calculated *TR* and $t_{abs}$ for fixed values of solar zenith angle, $q_o$ and $t_{ext}$ using AERONET individual almucantar inversions at GSFC in 2002-2003. We then fitted linear regression model, equation (1), to all calculated pairs (*TR*, $t_{abs}$) to estimate *TR* sensitivity selectively to $t_{abs}$, treating size distribution and real part of refractive index, $n_R$, effects as random errors (Figure 1).

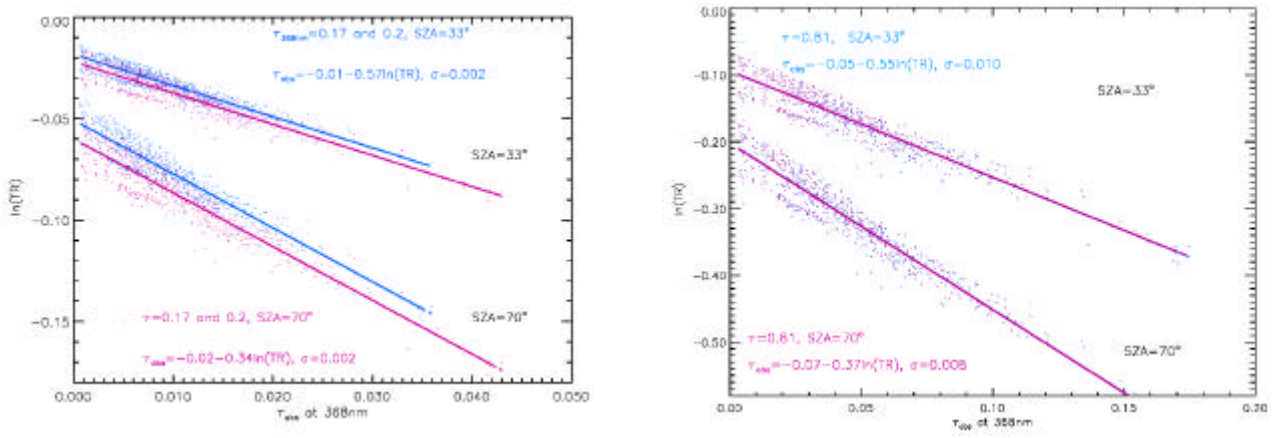


**Figure 1 Relationship between Rayleigh normalized total transmittance, TR and $t_{abs}$ at 368nm, assuming fixed $t_{ext}$=0.167 (red) and 0.2 (purple) and $q_o$=33°,70°. Linear regression model (1) is fitted to al data points assuming variability due to size distribution as random errors**

The regression coefficients quantify *TR* sensitivity to aerosol parameters as function of solar zenith angle (Table 1). The expected accuracy of $t_{abs}$ retrieval from MFRSR measurements is ~0.008-0.02 limited by the measured accuracy of total voltage ($V_T$) and calibration ($V_0$). The variability in aerosol size distribution and real refractive index becomes comparable to the measured uncertainties only for large aerosol loadings ($t_{ext}$>0.5). The measurement uncertainties (discussed in detail in the first paper[38]) and regression coefficients for high and low aerosol loadings are summarized in Table 1. We note that estimated retrieval uncertainties of $t_{abs}$ and ω for shadowband technique (Table 1) are comparable to almucantar technique[25-27] for favorable conditions (large

solar zenith angles, $q_o$ >45$^o$ and high aerosol loadings $t_{ext}$(440)>0.4). However, an important advantage of the shadowband technique is that it remains sensitive to $t_{abs}$ even at low solar zenith angles, when the almucantar technique is not sensitive to $t_{abs}$.[25-27] On the other hand, cosine correction errors increase for shadowband measurements at high solar zenith angles (see discussion in the first part), while cosine errors are absent for the CIMEL. Thus, the two types of measurements are required for measuring complete diurnal cycle of aerosol absorption.

## 4. PRACTICAL IMPLEMENTATION OF UV- MFRSR AEROSOL ABSORPTION RETRIEVAL

Cloud-screened[30] CIMEL sky radiance almucantar measurements at 440nm, 675nm, 870nm and 1020nm (downloaded from the web site: http://aeronet.gsfc.nasa.gov ) were used in conjunction with the direct sun–measured aerosol optical thickness $t_{ext}$ at these wavelengths to retrieve column average PSD and effective refractive index (real (n) and imaginary (k), independently at each wavelength) following the methodology of Dubovik and King[25]. Internally, homogeneous spherical particles with radii between 0.05 and 15 micron were assumed in the retrievals of PSD and effective refractive index. The refractive index was kept constant with particle radius and n was constrained between 1.33 and 1.6. Thus, the inversion allows estimation of spectral single scattering albedo, ω, and aerosol absorption optical thickness, $t_{abs}$ between 440 and 1020nm [26,27]. To extend these quantities into UV spectral range, additional measurements were conducted of diffuse and total irradiance by UV-MFRSR as well as column ozone measurements by the Brewer double spectrophotometer. These measurements were combined with a forward radiative transfer model to derive effective refractive index (imaginary part, k) as described below.

First, direct sun atmospheric transmittance was obtained from UV-MFRSR 3-minute diffuse ($V_F$) and total ($V_T$) voltage measurements and used in combination with interpolated/extrapolated AERONET $t_{ext}$ measurements to estimate zero air mass voltages, $V_o$ for each individual MFRSR measurement. Daily average $<V_o>$ estimates were obtained and used to derive $t_{ext}$ for every 3-min MFRSR measurement in each spectral channel as described in the first paper of the series[38].

Next, Brewer ozone and UV-MFRSR $t_{ext}$ measurements were used as input to the forward radiative transfer (RT) code[31] along with AERONET standard retrievals of the column-integrated PSD and the real part of refractive index at 440nm (available at http://aeronet.gsfc.nasa.gov) to infer an effective imaginary part of the UV aerosol refractive index (k). This was done by separately fitting the diffuse to direct ($DD=V_F/V_D$), diffuse fraction ($DT=V_F/V_T$) and total transmittance ($T=V_T/V_0$) MFRSR measurements to the calculated values separately for each spectral channel. The advantage of utilizing dimensionless ratios (*DD*, *DT* and *T*) is that radiometric calibration is not needed for the MFRSR, since the same detector measures both the total and diffuse flux. Agreement between all 3 methods provides a robust check on MFRSR calibration and correction for systematic measurement errors (i.e. angular and spectral response corrections).

Since a complete set of CIMEL almucantar measurements at 4 wavelengths takes about 5 minutes (and $\tau_{ext}$ from +/-16 minutes are used as input to the inversion), while MFRSR measurements were made at 3-minute intervals, we have analyzed all available MFRSR data within time interval +/-30min of each AERONET almucantar measurement. We assume that aerosol type does not change during this period and the only changes in radiation field arise from changes in solar zenith angle and aerosol optical thickness. Therefore, we use the same aerosol size distribution and real part of refractive index for any given 60-minute time slot, but allowed for $t_{ext}$ and $q_0$ changes in 3-minute increments. Then we switch to the next 60-minute time slot from the next available AERONET retrieval and use new aerosol-inverted parameters. If timeslots for 2 consecutive AERONET retrievals overlap, we repeat MFRSR fitting for all overlapping points with the new aerosol parameters. This provides us a test of sensitivity of our results to real time changes in AERONET inversion parameters (PSD and $n_R$) used as input to our fitting technique. We run the forward RT calculations in real time to fit every single 3-minute MFRSR measurement independently at each wavelength. The advantage of this approach is that forward RT calculations are always done for exact conditions of the measurement (solar zenith angle, $t_{ext}$, aerosol parameters), so no interpolation in solar angle or aerosol parameters (other than absorption coefficient) is involved.

The methodology of forward RT modeling and MFRSR ω retrieval is as follows:

1) Standard discrete AERONET column volume PSD in 22 size bins between 0.05μm and 15μm was first parameterized using bi-modal lognormal volume size distribution[27]. This parameterization requires 6 input parameters: column volume, modal radius and standard deviation separately for fine and coarse modes.
2) Volume PSD parameters were analytically converted to number column density parameters. Since we only need the shape of the PSD and not the absolute value, only five input parameters remain: modal radii and standard deviations separately for fine and coarse modes and the ratio of the total number of particles in fine and course modes. The implicit normalization occurs via specifying $t_{ext}$ equal to MFRSR measured $t_{ext}$.
3) Although our RT model does not require this, we assume the refractive index to be the same for fine and coarse modes (one component aerosol model) to be consistent with Dubovik and King inversion strategy[25]. Thus, following current AERONET assumptions, we seek to retrieve single effective refractive index, which is a weighted mean of the true column average refractive index over particle size distribution.
4) We assume the real part of refractive index, n, to be constant with wavelength, which is set to the AERONET retrieved value at 440nm. We believe this assumption will not result in a large retrieval error, since calculated direct irradiance is forced to be equal to the measured one via directly measured $t_{ext}$, while diffuse irradiance only weakly depends on the real part of refractive index[20,21].
5) We assumed an a-priori relative vertical profile of the aerosol loading in our forward model, which peaks in the boundary layer. The usual assumptions are that neither aerosol PSD nor the refractive index change with altitude[20,21]. No stratospheric aerosol was assumed. This a-priori aerosol profile was perturbed to test an assumption of vertically homogeneous atmosphere used in AERONET inversions[25-27] .

6) We assume horizontally homogeneous cloud-free atmospheric conditions. The cloud free portions of days were selected by visual examination and analysis of 3-minute irradiance series and all-sky camera images.
7) We use a single TOMS climatological ozone and temperature profile, which is scaled to the Brewer measured total column ozone amount for every actual MFRSR measurement. The Brewer total ozone amount compared well with TOMS ozone measurements that were used to fill in the missing Brewer ozone measurements. We currently do not assume any gaseous absorption other than ozone.
8) One of the main advantages the UV spectral region offers for aerosol measurements compared to the visible region is a uniformly low value of surface albedo of a few percent for snow free terrain. Therefore, we have manually excluded all days with even traces of partial snow cover from the current analysis. This allows us to use TOMS-derived climatologically snow-free value of surface albedo. This was verified with real-time EP-TOMS overpass reflectivity measurements at 360nm, corrected to the actual aerosol path radiance. We assume the surface albedo to be the same at all UV wavelengths (equal to 0.02)[32].
9) Accurately specifying surface pressure is an important requirement for radiation modeling in the UV spectral region. We used surface pressure measurements at nearby (5 km) USDA location in Beltsville, MD reduced by 4 mbar to account for change in altitude between Beltsville location (~30m asl) and GSFC UV-MFRSR location (roof of the building, ~100m asl according to our GPS measurements).
10) The ancillary measurements available at GSFC location allow us to constrain all required input to the Mie code and forward RT model, except the imaginary part of the aerosol refractive index, k, which is related to effective column aerosol absorption. We retrieve k at each wavelength by fitting either diffuse to direct ($DD=V_F/V_D$) or diffuse fraction ($DT=V_F/V_T$) or total transmittance ($T=V_T/V_0$) MFRSR measurements to the calculated values separately in each spectral channel. We do fitting iteratively, starting with AERONET derived $k_{440}$ as the initial value. We use the absolute value of the fitting residual as a measure of the goodness of the fit. In all results below the fit tolerance of 0.001 is assumed.
11) After a good fit is achieved, we regard $k_{368}$ as an effective fitting parameter, rather than microphysical particle property, because it accounts for all assumptions in our forward model as well as systematic measurements errors. On the other hand, derived radiative properties ($w_{368}$, $t_{abs}$) are less dependent on model assumptions; therefore, their errors should be smaller than errors in $k_{368}$ (see figure 1 and Table 1 for estimation of errors). Thus, the final value of $k_{368}$ along with the AERONET particle size distribution and $n_{440}$ was used to calculate single scattering albedo, $\omega_{368}$, using Lorentz-Mie code and $t_{abs}=(1-w_{368})t_{ext}$.
12) As an independent check, we conducted diffuse fraction fit using $w_{368}$ directly as input parameter to a different RT code (TUV4[4] based on DISORT [40] radiative transfer engine). Both $w_{368}$ retrievals agree well (within 0.01) provided correct value of asymmetry parameter was used as input to the TUV model. This check provides confidence that model assumptions and forward RT calculations are not the major source of error in our retrievals of $\omega_{368}$ and $t_{abs}$.

## 5. COMPARISON WITH AERONET $w_{440}$ ALMUCANTAR RETRIEVALS

Initially, we selected all CIMEL sky radiance almucantar measurements that were automatically cloud cloud-screened by the AERONET data system[30] and only looked at the days when AERONET inversions were available. Next, from these days we manually selected completely cloud-free conditions either in the morning or afternoon. For this manual cloud screening we used visual observations of sky as well as AERONET measurements of Angstrom exponent. We also filtered out days with partial snow cover. Thus, we focused on ~100 cloud-free portions of days between October 1, 2002 and March 1, 2004, meeting our cloud-free and snow- free criteria. To compare only high quality *w* retrievals we further selected periods with average $\tau_{ext}(440nm) > 0.3$ and used the Dubovik and King inversions[25,26] only for $\theta_o > 45^o$ while UV-MFRSR inversions for $\theta_o < 70^o$ to minimize cosine correction errors. These strict criteria leave us with only 15 summer days that were considered good for matchup comparisons (Table 2). For all cases we processed

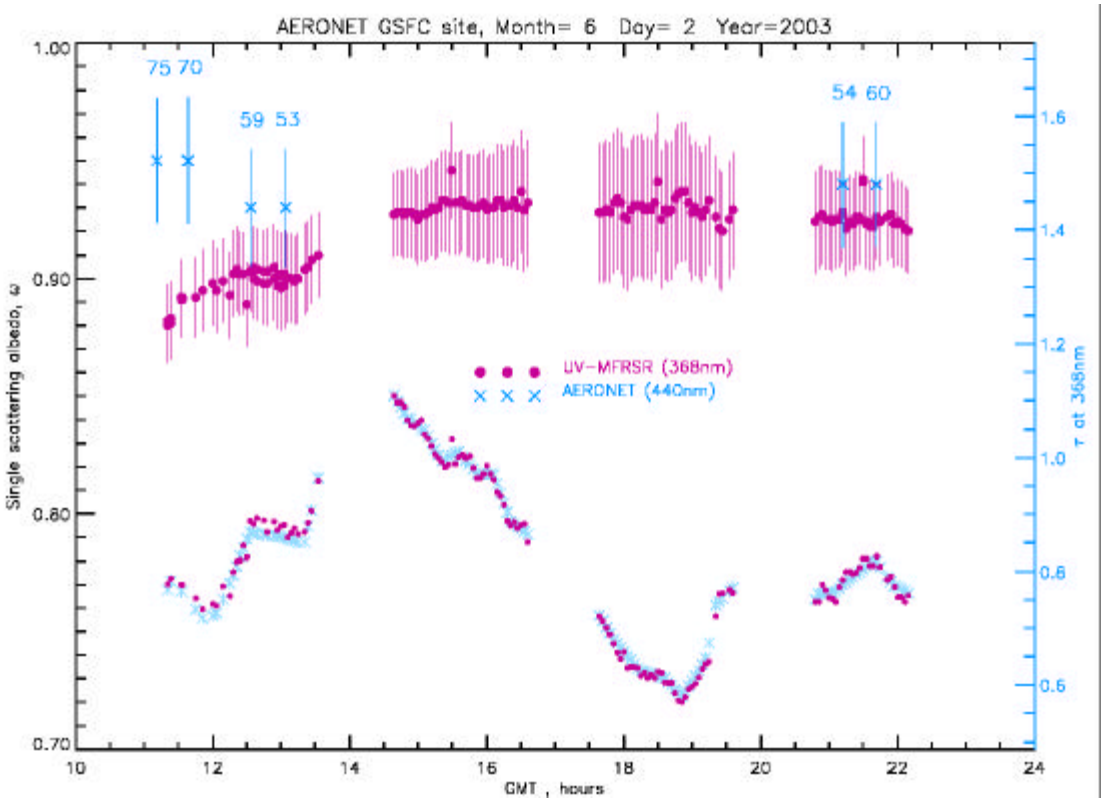


**Figure 2** MFRSR and AERONET single scattering albedo retrieval at GSFC on June 2 2003. The 3-minute MFRSR retrieved single scattered albedos at 368nm are shown as small purple spheres, while AERONET $\omega_{440}$ retrievals at 440nm are shown as large crosses with +/- 0.03 error bars[26]. The actual solar zenith angle was used in retrieval for each 3-min MFRSR measurement. The MFRSR assumptions were: surface albedo 0.02, Brewer measured total ozone, boundary layer aerosol profile and Dubovik and King[25]inverted particle size distribution within +/- 30min of each CIMEL almucantar measurement.

MFRSR data 3 times using different fitting parameters (diffuse/direct voltage ratio, diffuse/total voltage ratio and total normalized voltage $V_T/V_0$). We also compared with $w_{368}$ retrievals not using information from individual AERONET inversions, but assuming climatologically average asymmetry parameter in the TUV[4] forward radiative transfer code. We got essentially same $w_{368}$ retrievals (within 0.01) for all cases with high and low optical thickness. Selected case study results are shown in Figures 2-4. Table 2 compares ω retrieval results by both techniques using mean MFRSR retrievals averaged +/-30min of each individual AERONET inversion.

Figure 2 shows $w$ retrievals by both instruments on June 2 2003, when a long-range smoke plume was moving over GSFC location. The passage of the plume is evident from enhanced extinction optical thickness, $t_{368}$, measured by both instruments (shown on the right axis in figure 2). Visually, horizontal visibility remained high on this day with clear sight of horizon; however, the sky color was unusually white. According to 3-min MFRSR data, the most absorbing part of the smoke plume ($\omega_{368}$ ~0.88-0.9) was recorded in the morning (<14UT) with less absorbing $w_{368}$ ~0.93 for the rest of the day. Back trajectory analysis and satellite data suggested that the smoke plume was originated from fires in Siberia near lake Baikal. Physical-chemical processes during long-range transport of smoke can explain this relatively low absorption. Boreal forest smoke typically does not have low $w$ due to significant particle production from smoldering of woody fuels, which yields relatively small black carbon percentages. Also smoke particles tend to become less absorbing with age as the particle size increases due to coagulation during transport[36].

Although complete AERONET inversions are available for the whole day, we do not compare with $w_{440}$ retrievals for cases when solar zenith angle is less than 45$^o$, because the uncertainty in $w_{440}$ is significantly larger for these cases[26,27]. However, we use inverted particle size distribution results that were shown to be accurate for all conditions[26,27]. We also do not use MFRSR $\omega_{368}$ retrievals for cases when $\theta o > 75^o$, because the cosine-correction uncertainty for the measured diffuse irradiance is larger for these cases. The additional uncertainty at high solar zenith angles arises from using a pseudo-spherical version of the forward radiative transfer code, which corrects only direct sun irradiance, thus underestimating diffuse irradiance[31]. Thus, the two methods of estimating ω are complementary in that the Dubovik and King[25] retrieval requires large solar angles, while MFRSR data are more reliable at low solar zenith angles.

Table 2 quantifies different AERONET aerosol parameters on June 2 (day 153). The real part of refractive index at 440nm increased from 1.39 to 1.5 during smoke passage and decreased later to 1.46. The imaginary part of refractive index was higher in UV than in the visible ( $k_{368}$=0.014 - 0.02, $k_{440}$=0.007 – 0.013 ). The difference was larger than specified uncertainty for AERONET k retrievals (+/-0.003)[27] for all cases except one retrieval. These differences in k were consistent with lower ω values in UV ($\omega_{368}$=0.89-0.92 compare to $\omega_{440}$=0.93-0.95). This suggests that ω spectral dependence in the visible (lower ω at longer wavelengths)[27] flattens out and even reverses in UV. However, it is emphasized that, except for SZA>70$^o$ , the ω retrieved at 368nm and 440nm are within the range of overlap of retrieval uncertainties.

The Angstrom exponent was high and stable during the day ($\alpha_{440/870}$=1.73-1.88), suggesting predominantly fine-mode particles. However, the Angstrom exponent was smaller in UV ($\alpha_{380/440}$=0.73-0.82) compared to the visible wavelengths. This suggests substantial curvature of the ln(τ) vs ln(λ) dependence (α'=1.7-1.8)[24,29]. The cause of large ω discrepancy in the morning (~11.5UT) remains unknown.

We also studied sensitivity of $\omega_{368}$ results to assumed aerosol vertical profile. The smoke plume height over Eastern Shore in Maryland and Virginia was ~3km according to Lidar data (UMBC elastic lidar system (ELF) at Chesapeake Lighhouse, 36°54.6'N, 75°42.6' W)[33]. Therefore, we repeated MFRSR retrievals with aerosol height at 3km with essentially unchanged results. We found that MFRSR results are not sensitive to the smoke vertical profile (at least at 368nm).

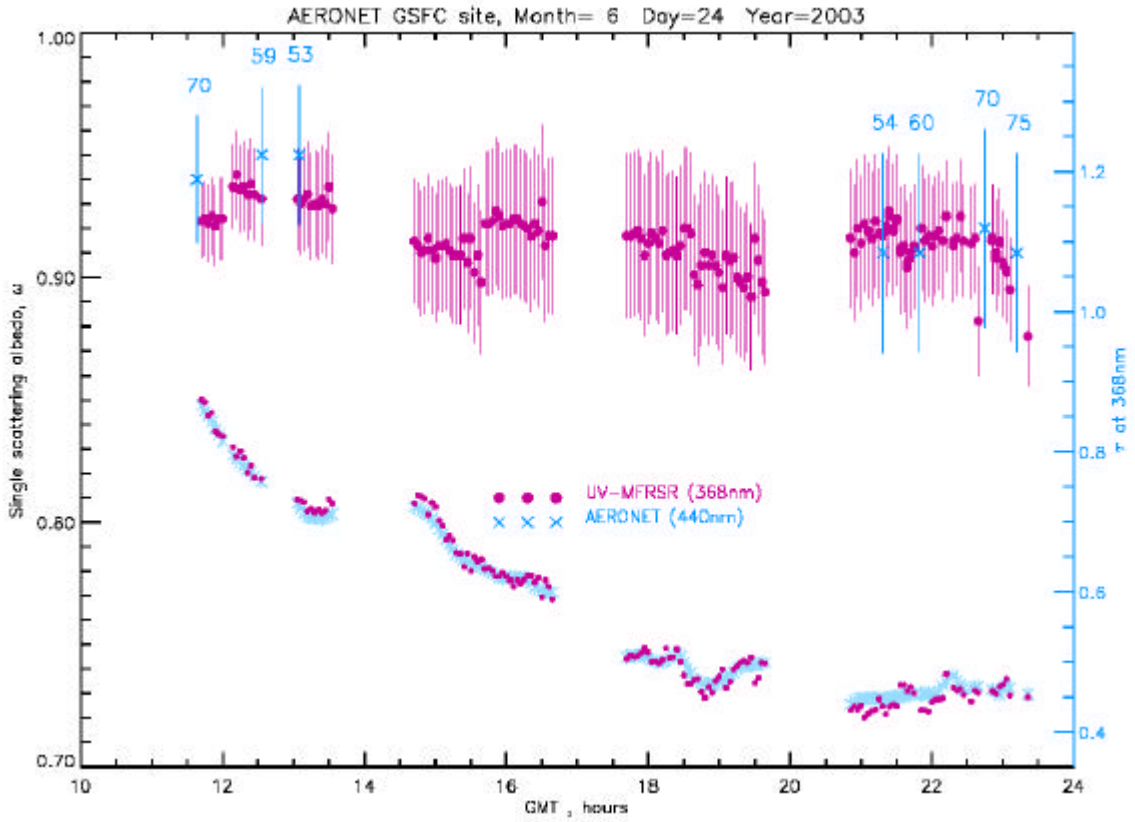


***Figure 3 same as figure 2, on June 24, 2003***.

**Figure 3** shows ω comparisons on June 24 2003, which was typical for a summer local ozone pollution episode. A high-pressure system over the Mid-Atlantic region for this week prevented air exchange; therefore tropospheric ozone pollution was building up as a result of local pollution (mostly traffic) and high solar insulation[3] (air quality public warning was "Code orange" on June 24). The conditions were mostly cloud-free for this day. In the morning aerosol absorption was

higher in UV, but differences were not significant. Aerosol extinction decreased during the day, while absorption increased slightly, but more rapidly in the visible. In the afternoon both retrievals show excellent agreement ($\omega_{368}$=0.91-0.92, $k_{368}$=0.011-0.014, $\omega_{440}$=0.91-0.92, $k_{440}$=0.01-0.012). AERONET real part of refractive index at 440nm changed between 1.39 and 1.59. The Angstrom exponent was much higher than for smoke event on June 2, especially in UV (Table 2, day 175) due to significantly smaller radius and broader σ of the fine mode on June 24.

We selected ω to demonstrate retrievals on August 25, 2003 (**Figure 4**) because of strong daily variation in $w_{368}$ with unusually low values ($w_{368}$ ~0.85) in the middle of the day. This case highlights the importance of measuring the complete diurnal cycle of summertime aerosol absorption, not just morning and afternoon periods.

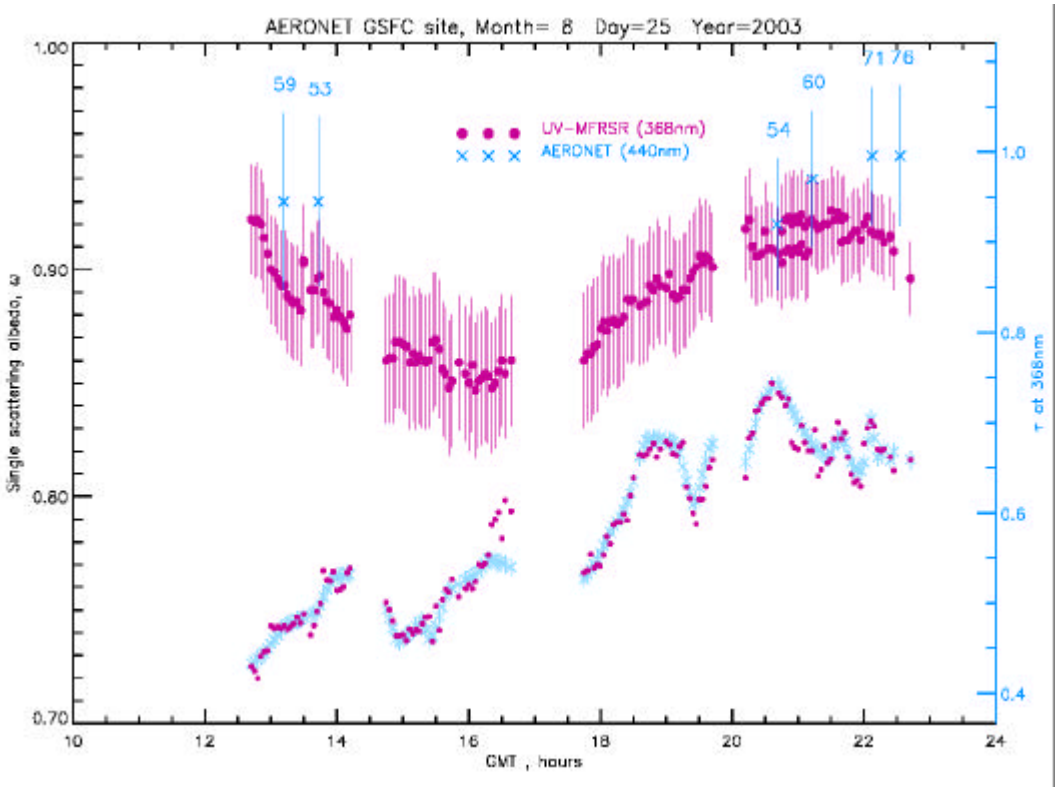


***Figure 4 same as figure 2, on August 25, 2003***.

As we mentioned in section 4, AERONET inversion of *PSD* and refractive index (real part at 440nm, $n_{440}$) within 30 minutes of the individual UV-MFRSR measurement is used as input to the UV-MFRSR forward RT model. If the 30min timeslots for 2 consecutive AERONET retrievals overlap, as in case of UV-MFRSR retrievals between 20.67UT and 21.2UT, we repeat UV-MFRSR fitting for all overlapping points with the new AERONET input aerosol parameters (from

21UT retrieval). In this particular example, *PSD's* were close for 2 consecutive AERONET retrievals ($R_{V,fine}$=0.14μm, $ln(s_{fine})$=0.381 at ~20.67UT versus $R_{Vfine}$=0.15μm, $ln(s_{fine})$=0.384 at ~21.2UT), but $n_{440}$ increased significantly, causing the asymmetry parameter, $g_{368}$, of the inverted aerosol phase function to decrease for the latter AERONET retrieval ($g_{368}$=0.735 using $n_{440}$=1.33 at ~20.5UT and $g_{368}$=0.676 using $n_{440}$ =1.56 at ~21UT). We could estimate the effect of changing $g_{368}$ on retrieved $w_{368}$ using the two-stream approximation[39] for total transmittance ($T_T$):

$$T_T \cong 1 - \frac{(1-g_{368})t_{ext}}{(1-g_{368})t_{ext} + 2m_o} \qquad (2)$$

According to equation (2) the decrease in $g_{368}$ (meaning less asymmetric phase function) would cause calculated $T_T(calc)$ to decrease for a non-absorbing aerosol layer with fixed $t_{ext}$ and solar zenith angle ($m_o=cos(q_o)$~0.5). Therefore, fitting the measured $T_T(meas)$ with this new $T_T(calc)$ would require less absorption or larger inverted $w_{368}$. The actual $w_{368}$ retrievals (figure 4) show that increase in input $n_{440}(=n_{368})$ does cause the increase in inverted $w_{368}$ in agreement with our estimate. We note that less pronounced jumps in $w_{368}$ retrievals caused by changing in AERONET input parameters can be also seen on other retrieval days and times (figures 3-4). However, the jumps were typically within the range of overlap of $w$ retrieval uncertainty, so we consider them practically insignificant until $w$ retrieval uncertainty will be close to ~0.01.

**Table 2** summarizes good comparisons cases (65 matchups) of ω retrievals using almucantar and shadowband techniques. Overall, ω was slightly lower in UV than in the visible: case average $<\omega_{368}>$=0.93 +/-0.02 (1σ) compared to $<\omega_{440}>$ =0.95 +/-0.02 (1σ). However, the differences ($<\omega_{440} - \omega_{368}>$ ~0.02, rms difference ~0.016) are smaller than uncertainties of both retrievals (~0.03). Low $<\omega_{368}>$ values are consistent with higher values for imaginary refractive index, k: $<k_{368}>$~0.01, $\sigma_{k368}$~0.004 compare to $<k_{440}>$~0.006, $\sigma_{k440}$~0.003. However, mean differences in $k$ ($<k_{368}-k_{440}>$~0.004, $\sigma_{k368-k440}$~0.003) were only slightly larger than AERONET retrieval uncertainty ~0.003[27].

In our opinion, $w_{368}$ retrieval results we report here (Table 2) do not allow the causes of apparent larger absorption at 368nm compare to 440nm to be separation with confidence. Continuing co-located measurements at GFSC location is important to improve the comparison statistics, but conducting these measurements at different sites with varying background aerosol conditions is also desirable. Limited number of previous ω retrievals in UV have revealed larger variability of ω at different locations[6,13]. Previous estimations of $w_{325}$ for Toronto, CA using Brewer spectrophotometer measurements ($w_{325}$ ~0.95 see Table 1 and figure 12 from Krotkov et al[6]) were slightly higher than $<w_{368}>$=0.93 at GSFC location. Similar $w$ retrievals using all channels of UV-MFRSR instrument were conducted at Black Mountain, NC[13]. The authors report $w_{368}$ ranging from 0.81 to 0.99 with the average value $<w_{368}>$=0.89 and estimated uncertainty +/-0.04 at $t_{ext}$~1.

It should be mentioned for AERONET wavelengths, that the ω increases with decreasing $l$ for fine mode smoke or pollution aerosol[27]. Therefore, the extrapolated differences in $w_{368}$ (predicted by AERONET) and $w_{368}$ retrieved by UV-MFRSR may be slightly greater than direct comparisons of $w_{440}$ to $w_{368}$. Therefore, it is important in the future to conduct similar measurement in locations affected by desert dust or more polluted sites, where UV aerosol absorption is expected to be higher.

## 5. UV-MFRSR RETRIEVAL RESULTS AT 368nm

Ultimately, our goal with UV-MFRSR measurements is to derive statistical distribution (daily and seasonal) of the absolute values and spectral dependence of UV absorption optical depth, $t_{abs}$ and single scattering albedo at urbanized region in the Eastern part of the US[3]. Figure 5 shows timeseries of $<t_{abs}(368)>$ for 17 months continuous monitoring at GSFC site.

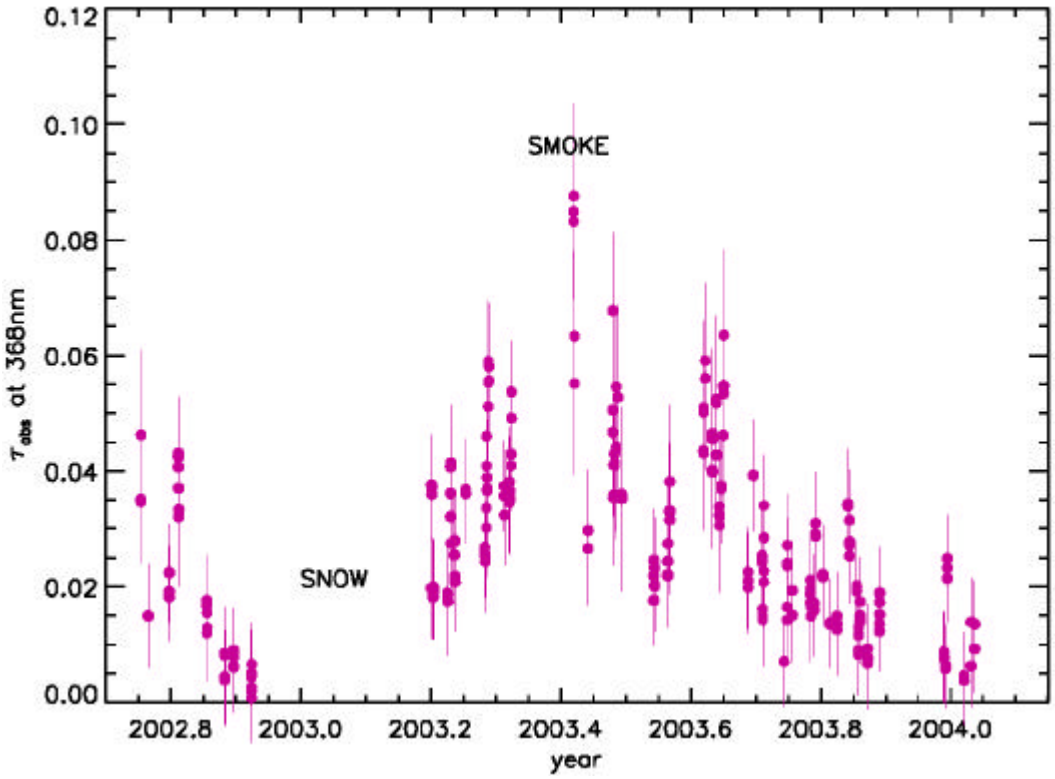


***Figure 5. Timeseries of aerosol absorption optical thickness $t_{abs}$ at 368nm, derived from 17 months UV-MFRSR operation at NASA GSFC site in Maryland, US. The data are for cloud-free and snow free conditions. Individual $t_{abs}(368)$ values were averaged over period of time +/-30min.The error bars of $t_{abs}(368)$ are interpolated by $t_{abs}(368)$ and solar zenith angle from estimates given in Table 1.***

The data gaps occurred due to unusually unfavorable weather conditions (rain or snow) in 2003. Still main features of the $t_{abs}$ seasonal cycle at GSFC can be seen from the figure: a pronounced summertime maximum with $t_{abs}(368)$~0.06-0.07 and wintertime minimum ~0.01. The maximum $t_{abs}$ typically occurs in summer due to combination of regional and local pollution sources with hot and humid weather conditions (summer haze). The weakly absorbing haze ($\omega_{368}$>0.9) is often associated with high levels of tropospheric ozone (ozone smog episodes)[3]. These summer haze conditions are responsible for summer high $t_{abs}$ values (at *368nm* ~0.06-0.07). Even on relatively clear summer days $t_{abs}$ is larger than ~0.02. On top of the annual cycle, occasional transient phenomena (long-range transport of biomass burning smoke and desert dust storms) can be clearly detected. One clear example is the passage of an aged smoke plume from Siberian forest fires over GSFC on June 2, 2003 (Figure 2), characterized by an unusually large $t_{abs}(368)$~*0.085*. Although occasional dust plumes had been reported at GSFC (April 2001 Asian dust plume), no dust events occurred during reported time period.

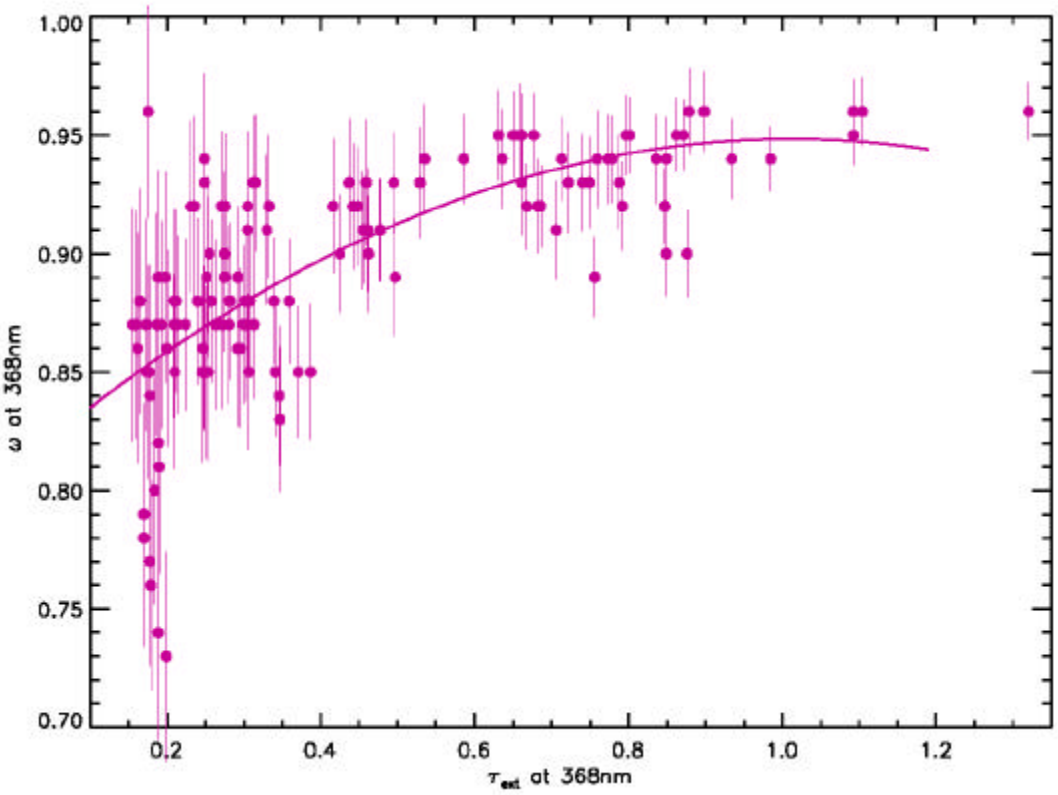


**Figure 6. Hourly average retrieved values < $w_{368}$ > as function of measured extinction optical thickness, $t_{abs}$ at 368nm for 17 months UV-MFRSR operation at NASA GSFC site in Maryland, US. The error bars are interpolated from Table 1 and are the same as for individual retrievals. We do not reduce error bars despite 1 hour averaging of individual retrievals, because retrieval errors are not believed to be random. Only < $w_{368}$ > values with estimated uncertainties less than 0.05 are shown.**

While the annual cycle in $t_{abs}$ is caused mainly by the annual cycle in aerosol extinction optical thickness, $t_{ext}$, the correlation between $t_{abs}$ and $t_{ext}$ is not perfect (linear correlation coefficient ~0.76 at 368nm), as would have been the case with no variability in aerosol single scattering albedo, $w=1-t_{abs}/t_{ext}$. Indeed, Figure 6 shows that $w_{368}$ is not constant, but decreases with decreasing $t_{ext}$. The downward $w$ trend is obvious from our data, despite progressively larger retrieval errors at small optical thickness. Indeed, AERONET $w_{440}$ results were reported at GSFC only for $t_{ext}(440)>0.4$[27], which would translate to $t_{ext}(368)\sim0.5$.

There are specific advantages in measuring aerosol absorption in UV that enable us to believe that our $w_{368}$ retrieval results down to $t_{ext}\sim0.2$: (1) the measured accuracy of AERONET reference instruments in the UV is perhaps better than the previously estimated value of ~0.01 at 340nm [29]; (2) the surface albedo is much smaller in UV than in the visible spectral region; (3) $t_{ext}$ is larger (for the same aerosol mass) than in the visible spectral range; (4) careful characterization of UV-MFRSR instrument, correction for known systematic errors, monitoring of instrument performance via daily CIMEL intercomparisons and characterizing atmospheric conditions; (5) stability and repeatability of individual $w_{368}$ retrievals; (6) ancillary and redundant aerosol measurements available at GSFC site. Indeed, measurement redundancy and instrument intercomparisons are key factors helping to push the limits of aerosol absorption measurements.

The decrease of single scattering albedo with optical thickness suggests that the type of aerosol changes between summer and winter conditions. It is well known that aerosol in the mid-Atlantic region in summer is strongly hydroscopic[35], therefore particle growth by swelling at high relative humidity may be partly the reason for reduced absorption in summer. Indeed, annual cycle of $w_{368}$ is the same as $t_{ext}$ annual cycle: with maximum in summer and minimum in winter. Obviously continuation of uninterrupted UV-MFRSR measurements at GSFC site is important to increase statistical significance of reported data.

Aerosol UV absorption results reported here have important implications for measuring UV surface irradiance from space. The relatively small $\tau_{abs}$ is difficult to detect from space using TOMS standard aerosol index (AI) method[6], especially when the aerosol is in the boundary layer (below 2 km). We calculated TOMS absorbing aerosol index to be negative for typical conditions at GSFC (except for smoke plumes in free troposphere). As a result, the TOMS UV algorithm would treat the aerosol as non-absorbing[6] overestimating surface UV irradiance by ~10%-20%[12]. Thus, the aerosol absorption could explain the average bias of TOMS UV estimate found in ground-based comparisons with the Canadian and US Brewer network[14] and needs to be incorporated in the future versions of the satellite surface irradiance algorithms.

## 6. CONCLUSIONS

We have demonstrated that an advantage of the shadowband technique is that the irradiance calibration can be established by calibrating the direct sun component and comparing with sun-photometers such as AERONET CIMELs. The shadowband method is complementary to the

Dubovik and King[25] almucantar retrieval of aerosol single scattering albedo, because the retrievals are more reliable at low solar zenith angles. Therefore, combined use of both instruments allows deriving the complete diurnal cycle of aerosol absorption. There are also advantages specific for the UV spectral region: (1) the surface albedo is much smaller in the UV than in the visible spectral region; (2) $t_{ext}$ is larger (for the same aerosol mass) than in the visible spectral range; (3) shorter wavelength UVB channels of UV-MFRSR are being used for measuring total ozone, which in turn is required for correction of aerosol measurements. Therefore, combined use of CIMEL sun and sky radiance measurements in the visible with MFRSR total and diffuse irradiance measurements in UV provide a important advantages for remote measurements of column aerosol absorption across the UV-Visible spectral range.

Inferred values of the effective UV imaginary refractive index were first used for comparisons of aerosol single scattering albedo, $w_{368}$, at 368nm and with AERONET retrievals at 440nm, $w_{440}$ using the Dubovik and King algorithm[25]. The measured small differences in absorption between 368nm and 440nm might suggest the presence of selectively UV absorbing aerosols[5] or interference from gases other than ozone[34]. However, the differences might also be caused by uncorrected systematic instrumental effects or absolute calibration uncertainties of sky radiances (~5% for almucantar technique[26]). In our opinion, the $\omega_{368}$ results we report here (Table 2) do not allow confident identification of the causes of apparent larger absorption at 368nm compared to 440nm. Continuing co-located measurements at GFSC location is important to improve the comparison statistics, but conducting these measurements at different sites with varying background aerosol conditions is also desirable. Qualitative changes in monitoring strategy would be also useful.

In the future we suggest:

1) Providing spectral overlap measurements for shadowband and almucantar techniques. This involves: absolute calibration of UV sky radiance channels of CIMEL instruments (340nm and 380nm) and extending almucantar inversion techique[25] to include UV sky scans. For the shadowband technique replacing filters in one or several channels of UV-MFRSR instrument to match those of CIMEL instrument will be also helpful;
2) Adding spectrometer measurements to separate between aerosol and gaseous absorption;
3) Conducting measurements at different sites with larger expected UV aerosol absorption[5] (more polluted sites with a higher black carbon fraction) or different types of aerosol (for sites with predominantly dust larger absorption is expected in UV than in the visible).

Using all cases for cloud-free days we derived the diurnal and seasonal dependence of aerosol absorption optical thickness, $t_{abs}$ at 368nm. The expected accuracy of $t_{abs}$ retrieval from MFRSR measurements is ~0.01 to 0.02 limited by the measured accuracy of total voltage ($V_T$) and calibration ($V_0$). The variability in aerosol size distribution and real refractive index becomes comparable to the measured uncertainties only for large aerosol loadings ($t_{ext}$>0.5). The $t_{abs}$ values show a pronounced seasonal dependence of $t_{ext}$ with maximum values $t_{abs}$ ~0.07 occurring in summer hazy conditions[3] and <0.02 in winter-fall seasons, when aerosol loadings are small.

We found that single scattering albedo decreases with decreases in extinction optical thickness. We believe that this behavior reflects real changes in the average aerosol composition between summer and winter month at the GSFC site. Indeed, the annual cycle of $w_{368}$ is the same to $t_{ext}$ annual cycle: with a maximum in summer and a minimum in winter. Obviously, continuation of uninterrupted UV-MFRSR measurements at the GSFC site is important to increase statistical significance of reported data.

**Acknowledgements**
The work was supported by NASA TOMS program We thank members of USDA UVB and NASA AERONET projects for their support.

## REFERENCES

1.O. Wild, X. Zhu, and M.J.Prather, " Fast-J: Accurate simulation of in- and below-cloud photolysis in tropospheric chemical models", *J. Atmos. Chem.*, **37**, 245-282, 2000.
2. M. Z. Jacobson, "Studying the effects of aerosols on vertical photolysis rate coefficient and temperature profiles over an urban airshed", *Journ. Geophys. Res.*, **103**, 10593-10604, 1998.
3. R.R. Dickerson, S. Kondragunta, G. stenchikov, K.L.Civerolo, B.G. Doddridge, and B.N.Holben, "The impact of aerosols on solar Ultraviolet radiation and photochemical smog", *Science* , 28, 827-830, 1997.
4. S. Madronich, *Environmental Effects of Ultraviolet (UV) Radiation*, chapter: UV radiation in the natural and perturbed atmosphere, *Lewis Publisher*, Boca Raton, 17-69, 1993.
5. M. Z. Jacobson, "Isolating nitrated and aromatic aerosols and nitrated aromatic gases as sources of ultraviolet light absorption", *Journ. Geophys. Res.*, **104**, 3527-3542, 1999.
6. N.A. Krotkov, P.K. Bhartia, J.R.Herman, V.Fioletov and J.Kerr, Satellite estimation of spectral surface UV irrdiance in the presence of tropospheric aerosols 1. Cloud-free case, *Journ. Geophys. Res*., 103, D8, 8779-8793, 1998.
7. A. Kylling, A. F. Bais, M. Blumthaler, J. Schreder, C.S. Zerefos, and E. Kosmidis, "Effect of aerosols on solar UV irradiances during the Photochemical activity and solar ultraviolet radiation campaign", *Journ. Geophys. Res.*, **103**, 26051-26060, 1998.
8. J. Reuder and H. Schwander, "Aerosol effects on UV radiation in nonurban regions", *Journ. Geophys. Res.*, **104**, 4065-4077, 1999.
9. J.R.Herman, N.Krotkov, E.Celarier, D.Larko, and G.Labow, "The distribution of UV radiation at the Earth's surface from TOMS measured UV-backscattered radiances," *J. Geophys. Res*., **104**, 12059-12076, 1999.
10. B. N. Wenny, V.K. Saxena, and J.E. Frederick, "Aerosol optical depth measurements and their impact on surface levels of ultraviolet-B radiation", *Journ. Geophys. Res.*, **106**, 17311-17319, 2001.
11. N.A. Krotkov, J.R.Herman, P.K. Bhartia, C. Seftor, Antti Arola, J. Kurola, S. Kalliscota, P. Taalas, I. Geogdzhaev, Version 2 TOMS UV algorithm: problems and enhancements, Opt. Eng. 41 (12) , 3028-3039, 2002.
12. N. A. Krotkov, J.R.Herman, P.K.Bhartia, C.Seftor, A.Arola, J.Kaurola, P.Taalas, I.Geogdzhaev, A. Vasilkov, OMI surface UV irradiance algorithm, P.Stammes (Ed.), vol. 3,

ATBD-OMI_03, version 2, 2002.
(http://eospso.gsfc.nasa.gov/eos_homepage/for_scientists/atbd/docs/OMI/ATBD-OMI-03.pdf ).

13. J.L.Petters, V.K. Saxena, J.R. Slusser, B.N. Wenny, and S. Madronich, "Aerosol single scattering albedo retrieved from measurements of surface UV irradiance and a radiative transfer model", *Journ. Geophys. Res*, 108 (D9) 4288, doi:10.1029/2002JD002360, 2003.
14. V. Fioletov, J.B.Kerr, D.I.Wardle, N. Krotkov, J.R. Herman, "Comparison of Brewer ultraviolet irradiance measurements with total ozone mapping spectrometer satellite retrievals", *Opt. Eng*. **41** (12) 3051-3061, 2002.
15. D.S. Bigelov, J.R. Slusser, A. F. Beaubien, and J. R. Gibson, "The USDA ultraviolet radiation monitoring program", *Bull. Amer. Meteor. Soc.*, **79**, 601-615, 1998.
16. L. Harrison, J. Michalsky, and J. Berndt, "Automated Multi-Filter Rotating Shadowband Radiometer: An instrument for Optical Depth and Radiation Measurements", *Appl. Optics*, **33**, 5118-5125, 1994.
17. L. Harrison and J. Michalsky, "Objective algorithms for the retrieval of optical depths from ground-based measurements", *Appl. Optics*, **33**, 5126-5132, 1994.
18. B.N. Holben et al., "AERONET – A federated instrument network and data archive for aerosol characterization", *Remote Sensing Environment*, 66, 1-16, 1998.
19. B.N. Holben et al., "An emerging ground-based aerosol climatology: Aerosol Optical Depth from AERONET", *Journ. Geophys. Res.*, **106**, 12 067-12 097, 2001.
20. B. M. Herman, S.R. Browning, J.J.DeLuisi, "Determination of the effective imaginary term of the complex refractive index of atmospheric dust by remote sensing: The diffuse-direct radiation method", *J. Atm. Sciences*, **32**, 918-925, 1975.
21. King, M. and B.M. Herman, "Determination of the ground albedo and the index of absorption of atmospheric particles by remote sensing. Part I: Theory", *J.Atmos. Sciences*, **36**, 163-173, 1979.
22. M. King, "Determination of the ground albedo and the index of absorption of atmospheric particles by remote sensing. Part II: Application", *J.Atmos. Sciences*, **36**, 1072-1083, 1979
23. T. F. Eck, B.N. Holben, I. Slutsker, and Alberto Setzer, "Measurements of irradiance attenuation and estimation of aerosol single scattering albedo for biomass burning aerosols in Amazonia", *J. Geophys. Res*., **103**, 31865-31878, 1998.
24. T. F. Eck, B.N.Holben, D.E. Ward, O. Dubovik, J.S. Reid, A. Smirnov, M.M. Mukelabai, N.C. Hsu, N.T. O'NeilL, and I. Slutsker, "Characterization of the optical properties of biomass burning aerosols in Zambia during the 1997 ZIBBEE field campaign", *Journ. Geophys. Res*., **106**, D4, 3425-3448, 2001.
25. O. Dubovik and M.D. King, "A flexible inversion algorithm for retrieval of aerosol optical properties from Sun and sky radiance measurements", *J. Geophys. Res* ., **105**, D16, 20673-20696, 2000.
26. O. Dubovik, A. Smirnov, B.N. Holben, M. D. King, Y. J. Kaufman, T. F. Eck, and I. Slutsker, "Accuracy assessments of aerosol optical properties retrieved from Aerosol Robotic Network (AERONET) Sun and sky radiance measurements", *J Geophys. Res*., **105**, D8, 9791-9806, 2000.
27. O. Dubovik, B.Holben, T.Eck, A. Smirnov, Y. J. Kaufman, M. D. King, D. Tanre, and I. Slutsker, Variability of Absorption and Optical properties of key aerosol types observed in worldwide locations, *J. Atmos. Sciences*, **59**, 590-608, 2002.

28. W. Gao et al., “Direct-sun column ozone retrieval by the ultraviolet multifilter rotating shadow-band radiometer and comparison with those from Brewer and Dobson spectrophotometers”, *Appl. Optics*, *40*, 3149-3155, 2001
29. T.F. Eck, B.N.Holben, J.S.Reid, O.Dubovik, A.Smirnov, N.T.O'Neill, I.Slutsker, and S.Kinne, Wavelength dependence of the optical depth of biomass burning, urban and desert dust aerosols, *Journ. Geophys. Res.*, **104**, 31333-31350, 1999.
30. A. Smirnov, B.N.Holben, T.F.Eck, O.Dubovik, and I. Slutsker, “Cloud screening and quality control algorithms for the AERONET data base”, *Rem. Sens. Env*., 73(3), 337-349, 2000
31. Herman, B. M., T. R. Caudill, D. E. Flittner, K. J. Thome, and A. Ben-David, A comparison of the Gauss-Seidel spherical polarized radiative transfer code with other radiative transfer codes, Appl. Opt, 34, 4563-4572, 1995.
32. J.R. Herman and E. Celarier, “Earth surface reflectivity climatology at 340 to 380 nm from TOMS data,” *J. Geophy. Res*., **102**, 28003-28011, 1997.
33. Hoff et al 2004, fall 2003 AGU presentation, 2003
34. A.N.Rublev, N.E.Chubarova, A.N. Trotsenko, and G.I. Gorchakov, Determination of $NO_2$ column amounts from AERONET data, Izvestiya, Atmospheric and Oceanic Physics, 40, 54-67, 2004.
35. R. Kotchenruther, R., and P.V. Hobbs, “Humidification factors of aerosols from biomass burning in Brazil”, *J. Geophys. Res*., 103, 32,081-32090, 1998.
36. T.F.Eck, et al,”High aerosol optical depth biomass burning events: A comparison of optical properties for different source regions”, *Geophys. Res. Let.*, 30(20), 2035, doi:10.1029/2003GL017861, 2003
**37.** H. Randriamiarisoa, P.Chazette, and G. Megie, “Retrieving the aerosol single-scattering albedo from the NO2 photolysis rate coefficient”, *Tellus*, 56B, 118-127, 2004
38. N.A. Krotkov, P.K. Bhartia, J.R.Herman, J. Slusser, G. Scott, G. Labow, T. F. Eck and B. N. Holben, “UV aerosol absorption experiment (2002-04): 1. UV-MFRSR calibration and performance at GSFC”, Opt. Eng., this issue, 2005
39. J. A., Jr., Coakley , and P.Chylek, “The two-stream approximation in radiative transfer: Including the angle of the incident radiation”, *J. Atmos. Sci*., 32,409-418, 1975
40. K. Stamnes, et al., Numerically stable algorithm for descrete-ordinate-method radiative transfer in multiple scattering and emitting layered media, *Appl. Opt., 27,* 2502-2509, 1988.

## Figure captions

**Figure 1** Relationship between Rayleigh normalized total transmittance, TR and $\tau_{abs}$ at 368nm, assuming fixed solar zenith angle $\theta_o$=33$^o$,70$^o$ and extinction optical thickness $\tau_{ext}$ (a) 0.167 (red) and 0.2 (purple) (b) $\tau_{ext}$=0.8(red) $\tau_{ext}$=0.82 (purple). Linear regression model (1) is fitted to al data points assuming variability due to size distribution as random error. Regression coefficients are given in Table 1.

**Figure 2** MFRSR and AERONET single scattering albedo retrieval at GSFC on June 2 2003. The 3-minute MFRSR retrieved single scattered albedos at 368nm are shown as small purple spheres, while AERONET $\omega_{440}$ retrievals at 440nm are shown as large crosses with +/- 0.03 error bars[26]. The actual solar zenith angle was used in retrieval for each 3-min MFRSR measurement. The MFRSR assumptions were: surface albedo 0.02, Brewer measured total ozone, boundary layer aerosol profile and Dubovik and King[25]inverted particle size distribution within +/- 30min of each CIMEL almucantar measurement.

**Figure 3** same as figure 2, on June 24, 2003
**Figure 4**. Same as Figure 2, on August 25, 2003

**Figure 5**. Timeseries of aerosol absorption optical thickness $\tau_{abs}$ at 368nm, derived from 17 months UV-MFRSR operation at NASA GSFC site in Maryland, US. The data are for cloud-free and snow free conditions. Individual $\tau_{abs}$(368) values were averaged over period of time +/- 30min.The error bars of $\tau_{abs}$(368) are interpolated by $\tau_{abs}$(368) and solar zenith angle from estimates given in Table 1.

**Figure 6.** Hourly average retrieved values $< \omega_{368} >$ as function of measured extinction optical thickness, $\tau_{abs}$ at 368nm for 17 months UV-MFRSR operation at NASA GSFC site in Maryland, US. The error bars are interpolated from Table 1 and are the same as for individual retrievals. We do not reduce error bars despite 1 hour averaging of individual retrievals, because retrieval errors are not believed to be random. Only $<w_{368}>$ values with estimated uncertainties less than 0.05 are shown.

***Table 1 MFRSR measurement errors, sensitivity to $t_{abs}$ for different conditions and expected retrieval errors***

| Sources of measured errors in MFRSR 368nm channel | τ=0.2 | | τ=0.8 | |
|---|---|---|---|---|
| | θ=33 | θ=70 | θ=33 | θ=70 |
| | Daily $V_0$ calibration error, $s_{\ln V_0}$ | | | |
| ΔlnV0 ( V0~2100mv) 1) $s_{\ln V_0}$ | 0. 01 (0.05) | 0. 01 (0.05) | 0. 02 (0.1) | 0.02 (0.1) |
| | Combined *TR* measurement and calibration errors | | | |
| Combined *TR* measurement error: $s_{\ln(TR)}$ 2) | ~0.022 (0.05) | ~0.022 (0.05) | ~0.036 (0.1) | ~0.036 (0.1) |
| | Measurement sensitivity: $\frac{\partial \ln(V_T)}{\partial(t_y)}$ | | | |
| Sensitivity ln(VT/V0) to $\tau_{abs}$ | 1.8 | 2.9 | 1.8 | 2.7 |
| Sensitivity ln(VT/V0) to $\tau_{ext}$ | 0.1 | 0.17 | 0.1 | 0.17 |
| | Expected retrieval errors | | | |
| Expected error in $\tau_{abs}$ due to measurement error, 1σ | 0.01 (0.03) | 0.007 (0.02) | 0.02 (0.05) | 0.013 (0.05) |
| Expected error in $\tau_{abs}$ due to uncertainty in PSD, 1σ 3) | 0.006 | 0.003 | 0.01 | 0.01 |
| Combined error in $\tau_{abs,}$ 1σ | 0.012 (0.03) | 0.008 (0.02) | 0.022 (0.051) | 0.016 (0.05) |
| Error in ω~ $\frac{\Delta t_{abs}}{t_{ext}}$ 4) | 0.06 (0.15) | 0.04 (0.10) | 0.03 (0.06) | 0.02 (0.06) |

1) AERONET V0 uncertainty for reference instruments combined with calibration transfer error (see part1 paper); 2)Assuming that calibration and *VT* measurement errors are uncorrelated (see paper 1); (3) The scatter of points around regression line gives retrieval noise if size distribution information is not used in $\tau_{abs}$ retrieval $\omega=1-\tau_{abs/\tau}\tau_{ext}$, assuming constant $\sigma_{\tau ext}$~0.01 and errors in extinction and absorption are uncorrelated

Table 2 Comparison of individual ω retrievals

| Year | DOY | UTC | <sza> | <aot $_{368}$> | N | <W $_{368}$> | <K $_{368}$> *10 $^{3}$ | aot $_{440}$ | W$_{440}$ | K $_{440}$ *10 $^{3}$ | n$_{440}$ | a $_{380440}$ | a $_{440870}$ | a' |
|---|---|---|---|---|---|---|---|---|---|---|---|---|---|---|
| 2002 | 275 | 12.4 | 71.5 | 0.586 | 5 | 0.94 | 7.9 | 0.441 | 0.98 | 2.5 | 1.33 | 1.28 | 1.78 | 1.04 |
| | 275 | 12.9 | 68.9 | 0.608 | 14 | 0.94 | 8.3 | 0.477 | 0.98 | 2.1 | 1.33 | 1.26 | 1.78 | 1.06 |
| | 275 | 15 | 52.1 | 0.661 | 12 | 0.93 | 10.8 | 0.525 | 0.96 | 5.7 | 1.37 | 1.27 | 1.81 | 1.1 |
| | 296 | 14.9 | 57.3 | 0.529 | 20 | 0.93 | 8.8 | 0.425 | 0.96 | 3.5 | 1.34 | 1.38 | 1.75 | 0.64 |
| | 296 | 15.9 | 52.3 | 0.459 | 16 | 0.93 | 10.1 | 0.349 | 0.97 | 3.5 | 1.54 | 1.46 | 1.78 | 0.46 |
| | 296 | 16.9 | 50.6 | 0.416 | 16 | 0.92 | 10 | 0.325 | 0.94 | 6 | 1.33 | 1.49 | 1.81 | 0.46 |
| 2003 | 153 | 11.2 | 71.9 | 0.782 | 2 | 0.89 | 19.9 | 0.678 | 0.95 | 7.1 | 1.39 | 0.82 | 1.7 | 1.82 |
| | 153 | 11.6 | 68.5 | 0.756 | 6 | 0.89 | 17.9 | 0.655 | 0.95 | 7.8 | 1.39 | 0.77 | 1.68 | 1.83 |
| | 153 | 12.6 | 58.9 | 0.849 | 16 | 0.9 | 19.7 | 0.763 | 0.93 | 12.7 | 1.46 | 0.73 | 1.68 | 1.88 |
| | 153 | 13.1 | 54.5 | 0.876 | 13 | 0.9 | 19.4 | 0.75 | 0.93 | 13 | 1.5 | 0.74 | 1.69 | 1.85 |
| | 153 | 21.2 | 55.5 | 0.788 | 18 | 0.93 | 14.3 | 0.671 | 0.94 | 11.7 | 1.49 | 0.74 | 1.66 | 1.75 |
| | 153 | 21.7 | 60 | 0.792 | 19 | 0.92 | 13.7 | 0.692 | 0.94 | 9.6 | 1.46 | 0.78 | 1.67 | 1.73 |
| | 174 | 21.3 | 50.5 | 0.408 | 2 | 0.89 | 13.8 | 0.312 | 0.92 | 8.6 | 1.35 | 1.42 | 1.85 | 1.08 |
| | 175 | 11.6 | 67.7 | 0.847 | 7 | 0.92 | 14.2 | 0.711 | 0.94 | 9.7 | 1.46 | 1.11 | 1.81 | 1.57 |
| | 175 | 12.6 | 61.3 | 0.778 | 9 | 0.94 | 12.5 | 0.615 | 0.95 | 10 | 1.59 | 1.19 | 1.84 | 1.47 |
| | 175 | 13.1 | 52.2 | 0.722 | 7 | 0.93 | 13.6 | 0.582 | 0.95 | 10.7 | 1.59 | 1.2 | 1.84 | 1.45 |
| | 175 | 21.3 | 54.8 | 0.442 | 17 | 0.92 | 11.2 | 0.341 | 0.91 | 10 | 1.36 | 1.51 | 1.93 | 1.04 |
| | 175 | 21.8 | 60.1 | 0.448 | 18 | 0.92 | 11.6 | 0.343 | 0.91 | 11 | 1.38 | 1.56 | 1.93 | 0.84 |
| | 175 | 22.7 | 68.8 | 0.456 | 9 | 0.91 | 12.5 | 0.344 | 0.92 | 9.7 | 1.39 | 1.62 | 1.93 | 0.62 |
| | 175 | 23.2 | 72.3 | 0.456 | 2 | 0.91 | 13.7 | 0.345 | 0.91 | 12.2 | 1.43 | 1.58 | 1.92 | 0.66 |
| | 176 | 11.2 | 71.4 | 0.477 | 5 | 0.91 | 13.4 | 0.351 | 0.93 | 8.5 | 1.4 | 1.78 | 2.02 | 0.3 |
| | 176 | 11.6 | 69 | 0.478 | 13 | 0.91 | 13.4 | 0.349 | 0.93 | 8.5 | 1.42 | 1.8 | 2.02 | 0.24 |
| | 176 | 12.6 | 59.4 | 0.455 | 17 | 0.91 | 14.3 | 0.313 | 0.94 | 8.3 | 1.44 | 1.8 | 1.98 | 0.13 |
| | 176 | 13.1 | 54.9 | 0.461 | 15 | 0.91 | 11.6 | 0.339 | 0.92 | 8.1 | 1.36 | 1.83 | 2.01 | 0.3 |
| | 177 | 11.6 | 67.7 | 1.092 | 4 | 0.95 | 6.7 | 0.792 | 0.96 | 4.6 | 1.4 | 1.73 | 2.2 | 0.89 |
| | 177 | 12.6 | 59.7 | 1.092 | 18 | 0.96 | 6.3 | 0.794 | 0.96 | 5.5 | 1.4 | 1.74 | 2.21 | 0.93 |
| | 177 | 13.1 | 54.8 | 1.104 | 15 | 0.96 | 6.4 | 0.825 | 0.96 | 5.3 | 1.42 | 1.74 | 2.21 | 0.96 |
| | 178 | 11.2 | 71.3 | 1.115 | 2 | 0.95 | 7.4 | 0.893 | 0.97 | 3.5 | 1.35 | 1.07 | 1.85 | 1.75 |

| | | | | | | | | | | | | | | |
|---|---|---|---|---|---|---|---|---|---|---|---|---|---|---|
| 2003 | 180 | 11.2 | 70.3 | 0.909 | 2 | 0.96 | 5.6 | 0.747 | 0.97 | 4.4 | 1.33 | 1.03 | 1.71 | 1.58 |
| 2003 | 180 | 11.7 | 67.5 | 0.899 | 11 | 0.96 | 5 | 0.753 | 0.97 | 4.2 | 1.33 | 1.02 | 1.7 | 1.55 |
| 2003 | 180 | 12.6 | 59.3 | 0.898 | 18 | 0.96 | 5.5 | 0.751 | 0.96 | 5.9 | 1.34 | 1.02 | 1.69 | 1.57 |
| 2003 | 180 | 13.1 | 54.6 | 0.879 | 15 | 0.96 | 6.3 | 0.737 | 0.97 | 4.9 | 1.38 | 1.02 | 1.69 | 1.58 |
| 2003 | 207 | 11.5 | 70.9 | 0.662 | 5 | 0.95 | 6.4 | 0.501 | 0.98 | 1.9 | 1.33 | 1.59 | 2.03 | 1.05 |
| 2003 | 207 | 11.9 | 68.5 | 0.631 | 13 | 0.95 | 6.5 | 0.494 | 0.98 | 2.5 | 1.33 | 1.59 | 2.02 | 1.06 |
| 2003 | 207 | 12.8 | 59.5 | 0.636 | 20 | 0.94 | 7.6 | 0.472 | 0.97 | 3.1 | 1.33 | 1.63 | 2.05 | 1 |
| 2003 | 207 | 13.3 | 54.9 | 0.658 | 16 | 0.95 | 7.5 | 0.522 | 0.95 | 6.7 | 1.33 | 1.58 | 2.03 | 1.06 |
| 2003 | 226 | 11.7 | 70.8 | 0.871 | 4 | 0.95 | 6.6 | 0.755 | 0.98 | 3 | 1.33 | 0.93 | 1.66 | 1.7 |
| 2003 | 226 | 12.1 | 68.4 | 0.862 | 12 | 0.95 | 7 | 0.741 | 0.98 | 2.4 | 1.33 | 0.95 | 1.66 | 1.69 |
| 2003 | 226 | 13 | 60 | 0.849 | 19 | 0.94 | 7.7 | 0.725 | 0.95 | 7.1 | 1.33 | 1.02 | 1.71 | 1.64 |
| 2003 | 226 | 13.6 | 55 | 0.836 | 13 | 0.94 | 8.1 | 0.712 | 0.95 | 6.3 | 1.33 | 1.01 | 1.7 | 1.64 |
| 2003 | 227 | 12.1 | 68.1 | 0.985 | 10 | 0.94 | 8 | 0.848 | 0.96 | 4.9 | 1.35 | 1.09 | 1.71 | 1.45 |
| 2003 | 227 | 13.6 | 54.9 | 0.934 | 14 | 0.94 | 8.5 | 0.768 | 0.96 | 5.1 | 1.36 | 1.1 | 1.73 | 1.5 |
| 2003 | 231 | 11.8 | 70.7 | 0.801 | 4 | 0.95 | 5 | 0.669 | 0.97 | 3.3 | 1.34 | 1.2 | 1.73 | 1.33 |
| 2003 | 231 | 12.2 | 68.2 | 0.797 | 12 | 0.95 | 7.4 | 0.647 | 0.98 | 2.1 | 1.33 | 1.25 | 1.77 | 1.33 |
| 2003 | 231 | 13.1 | 59.9 | 0.774 | 16 | 0.94 | 9 | 0.631 | 0.98 | 2.2 | 1.35 | 1.28 | 1.79 | 1.3 |
| 2003 | 231 | 13.6 | 54.3 | 0.759 | 13 | 0.94 | 8.2 | 0.615 | 0.95 | 5.8 | 1.33 | 1.24 | 1.71 | 1.3 |
| 2003 | 233 | 12.2 | 68.3 | 0.713 | 13 | 0.94 | 7.4 | 0.606 | 0.97 | 3.8 | 1.33 | 0.87 | 1.5 | 1.56 |
| 2003 | 233 | 13.1 | 59.7 | 0.749 | 20 | 0.93 | 8.9 | 0.64 | 0.97 | 4.1 | 1.33 | 0.81 | 1.47 | 1.64 |
| 2003 | 233 | 13.7 | 55.1 | 0.74 | 14 | 0.93 | 9.6 | 0.634 | 0.95 | 6.5 | 1.33 | 0.84 | 1.48 | 1.6 |
| 2003 | 235 | 11.8 | 71 | 0.677 | 6 | 0.95 | 6.5 | 0.649 | 0.99 | 0.8 | 1.39 | 1 | 1.58 | 1.41 |
| 2003 | 235 | 12.2 | 69.2 | 0.65 | 11 | 0.95 | 6.7 | 0.55 | 0.96 | 4.1 | 1.33 | 1.1 | 1.62 | 1.32 |
| 2003 | 235 | 13.2 | 59 | 0.535 | 17 | 0.94 | 8.3 | 0.457 | 0.94 | 7.3 | 1.33 | 1.18 | 1.64 | 1.21 |
| 2003 | 235 | 13.7 | 54.5 | 0.437 | 16 | 0.93 | 10.6 | 0.297 | 0.93 | 9.1 | 1.39 | 1.39 | 1.66 | 1 |
| 2003 | 237 | 13.2 | 60 | 0.462 | 19 | 0.9 | 11.1 | 0.366 | 0.93 | 5.8 | 1.33 | 1.5 | 1.67 | 0.45 |
| 2003 | 237 | 13.7 | 54.4 | 0.497 | 16 | 0.89 | 13.6 | 0.394 | 0.93 | 5.9 | 1.33 | 1.49 | 1.72 | 0.62 |
| 2003 | 237 | 20.7 | 55.3 | 0.706 | 17 | 0.91 | 10.7 | 0.557 | 0.92 | 7.4 | 1.33 | 1.57 | 1.87 | 0.82 |
| 2003 | 237 | 21.2 | 60.9 | 0.682 | 20 | 0.92 | 14.3 | 0.504 | 0.94 | 9.1 | 1.56 | 1.61 | 1.91 | 0.81 |
| 2003 | 237 | 22.1 | 69.3 | 0.668 | 13 | 0.92 | 12.1 | 0.497 | 0.95 | 5.7 | 1.4 | 1.72 | 1.98 | 0.66 |

1) Year
2) Day of Year
3) UT time of ARONET inversion data record (CIMEL almucantar scan includes 2 azimuthal scans of left and right hemispheres repeated at each wavelength ( 440nm, 675nm, 870nm, 1020nm)
4) MFRSR averaged $\theta_o$ +/-30min of AERONET inversion time
5) MFRSR $\tau_{368}$ averaged +/-30min of AERONET recorded inversion time
6) Number of MFRSR measurements averaged
7) MFRSR average $w$ at 368nm
8) MFRSR average imaginary part of column average effective refractive index, $10^3 \langle k_{368} \rangle$
9) AERONET measured $\tau_{ext}$ at 440nm
10) AERONET retrieved $w$ at 440nm using $\tau_{ext}$ at 440nm
11) AERONET retrieved imaginary part of column average effective refractive index, $10^3 \langle k_{440} \rangle$
12) AERONET retrieved real part of column average effective refractive index, $10^3 \langle n_{440} \rangle$
13) Angstrom parameter using AERONET measured $\tau_{ext}$ at 380nm and 440nm
14) Angstrom parameter using AERONET measured $\tau_{ext}$ at 440nm and 870nm

Second derivative of $\ln(\tau_{ext})$ versus $\ln(\lambda)$ defined as $-2C_2$, where C2 is coefficient of the second order polynomial fit to the measured $\tau_{ext}$ at 380nm, 440nm, 500nm, 675nm and 870nm

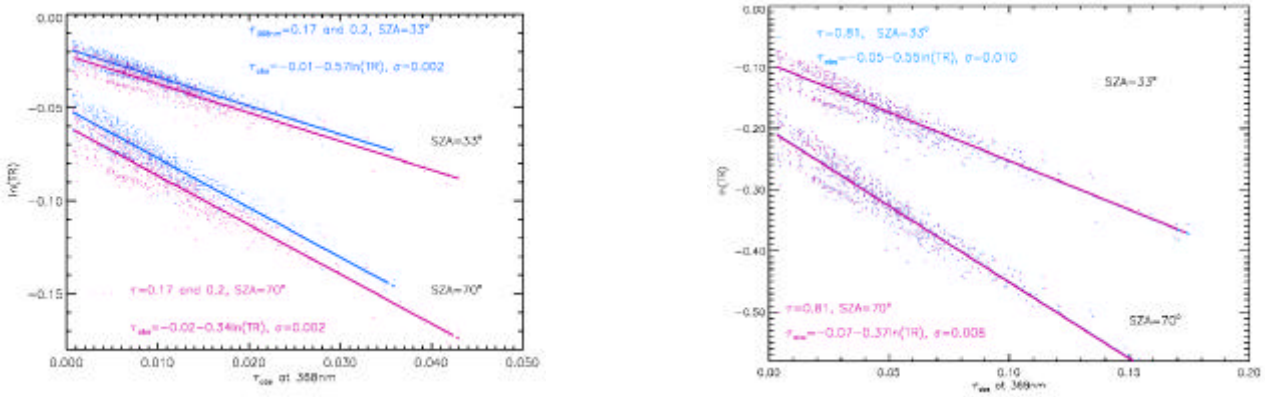


**Figure 1** *1 Relationship between Rayleigh normalized total transmittance, TR and $t_{abs}$ at 368nm, assuming fixed $t_{ext}$=0.167 (red) and 0.2 (purple) and $q_o$=33$^o$,70$^o$. Linear regression model (1) is fitted to al data points assuming variability due to size distribution as random errors*

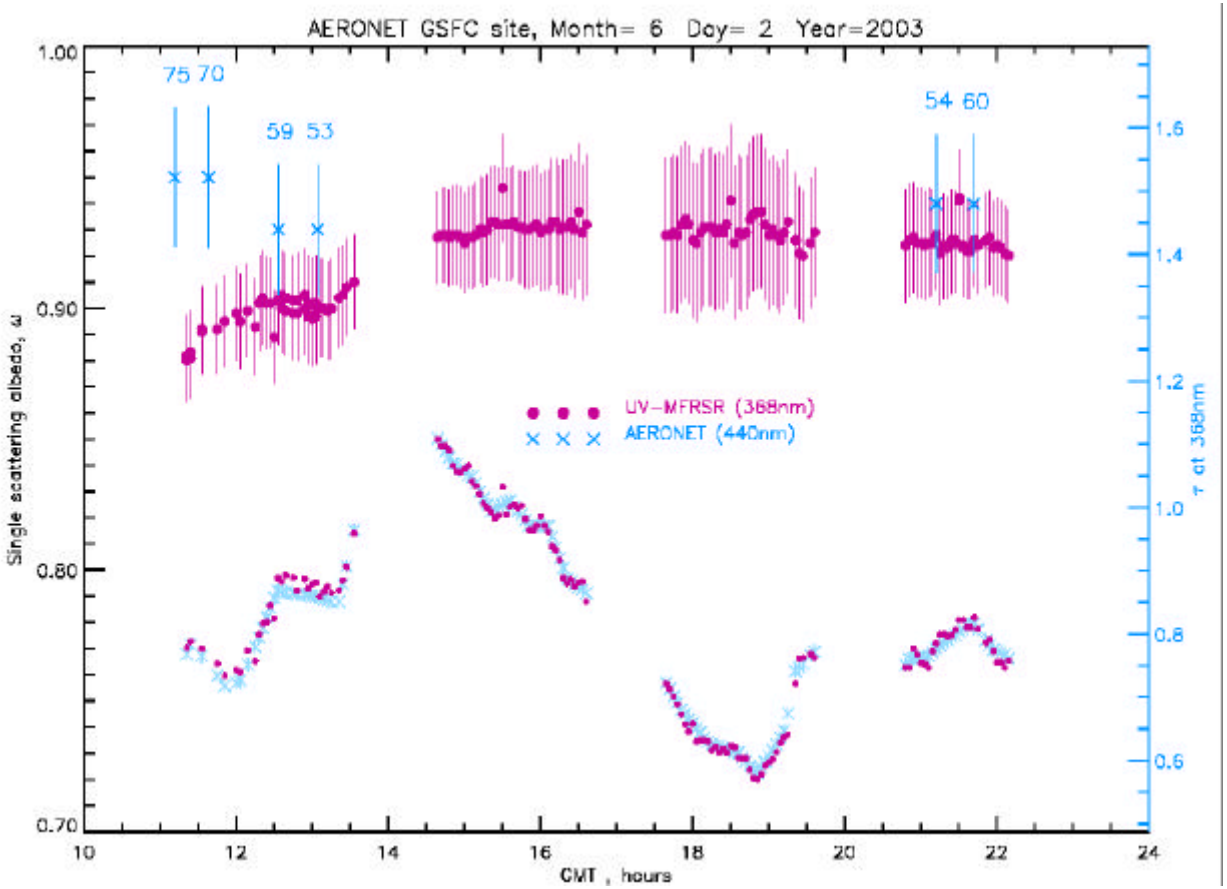


**Figure 2** MFRSR and AERONET single scattering albedo retrieval at GSFC on June 2 2003. The 3-minute MFRSR retrieved single scattered albedos at 368nm are shown as small purple spheres, while AERONET $\omega_{440}$ retrievals at 440nm are shown as large crosses with +/- 0.03 error bars[26]. The actual solar zenith angle was used in retrieval for each 3-min MFRSR measurement. The MFRSR assumptions were: surface albedo 0.02, Brewer measured total ozone, boundary layer aerosol profile and Dubovik and King[25]inverted particle size distribution within +/- 30min of each CIMEL almucantar measurement.

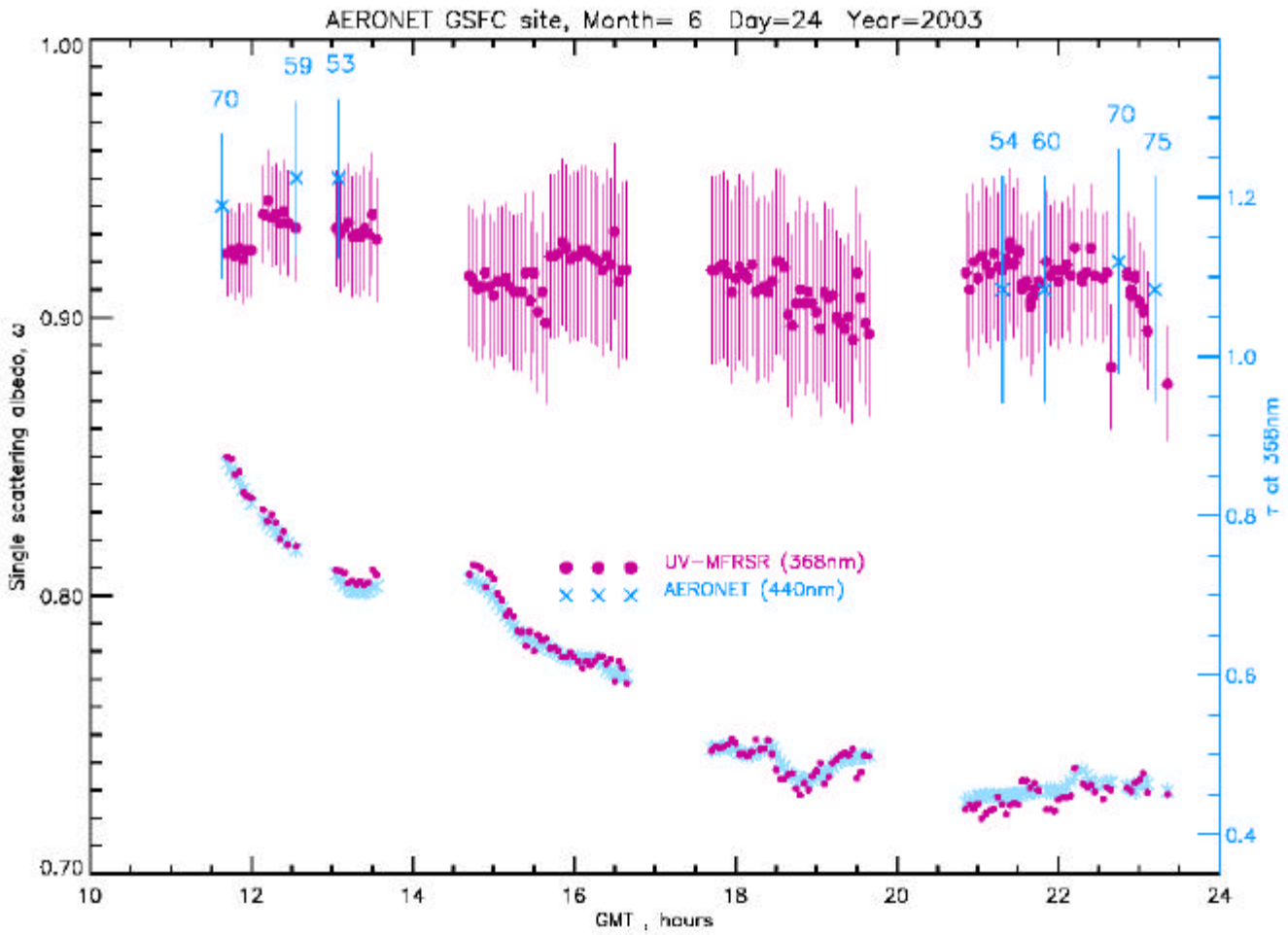


***Figure 3 same as figure 2, on June 24, 2003***

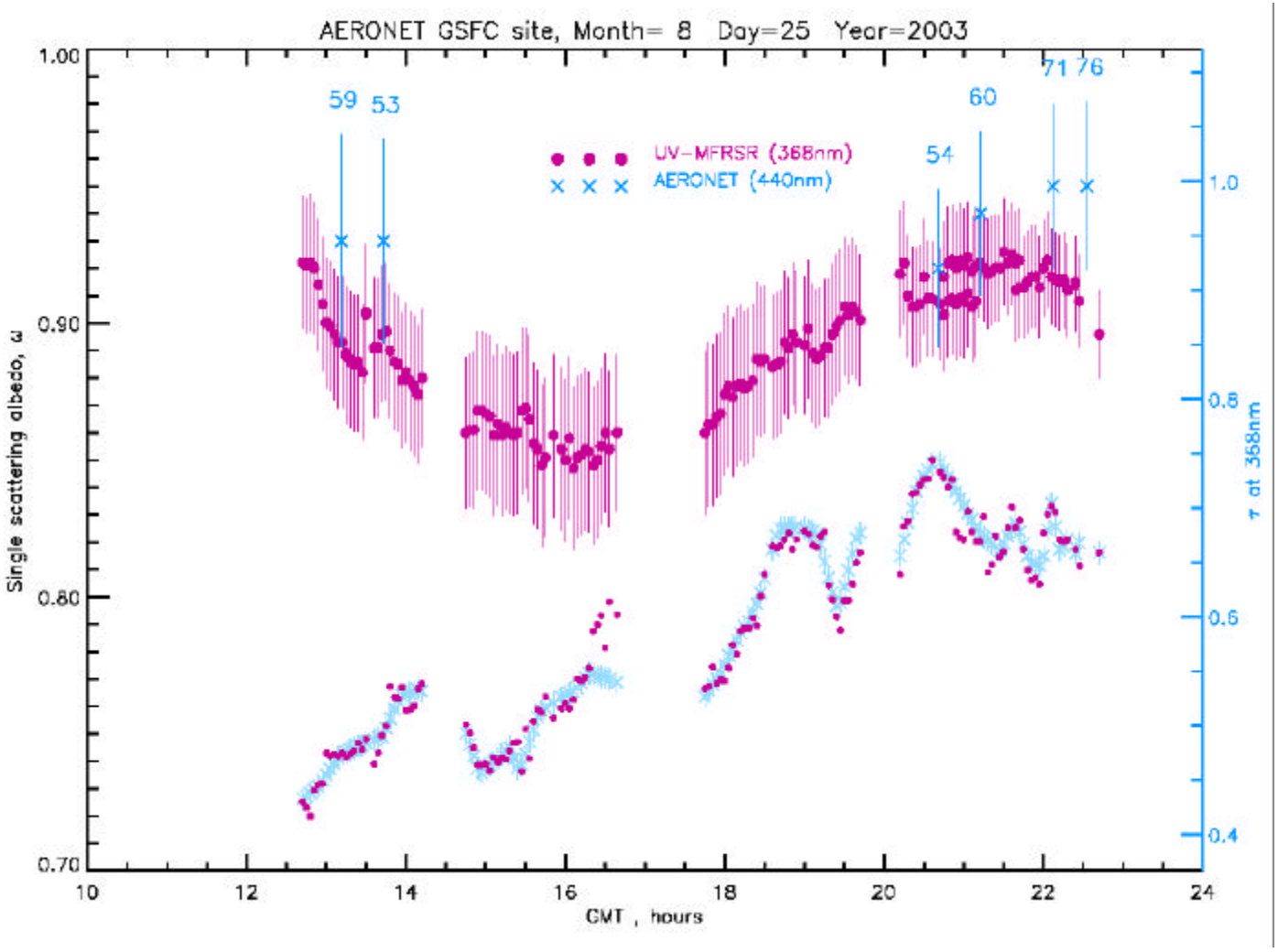


***Figure 4. Same as Figure 2, on August 25, 2003.***

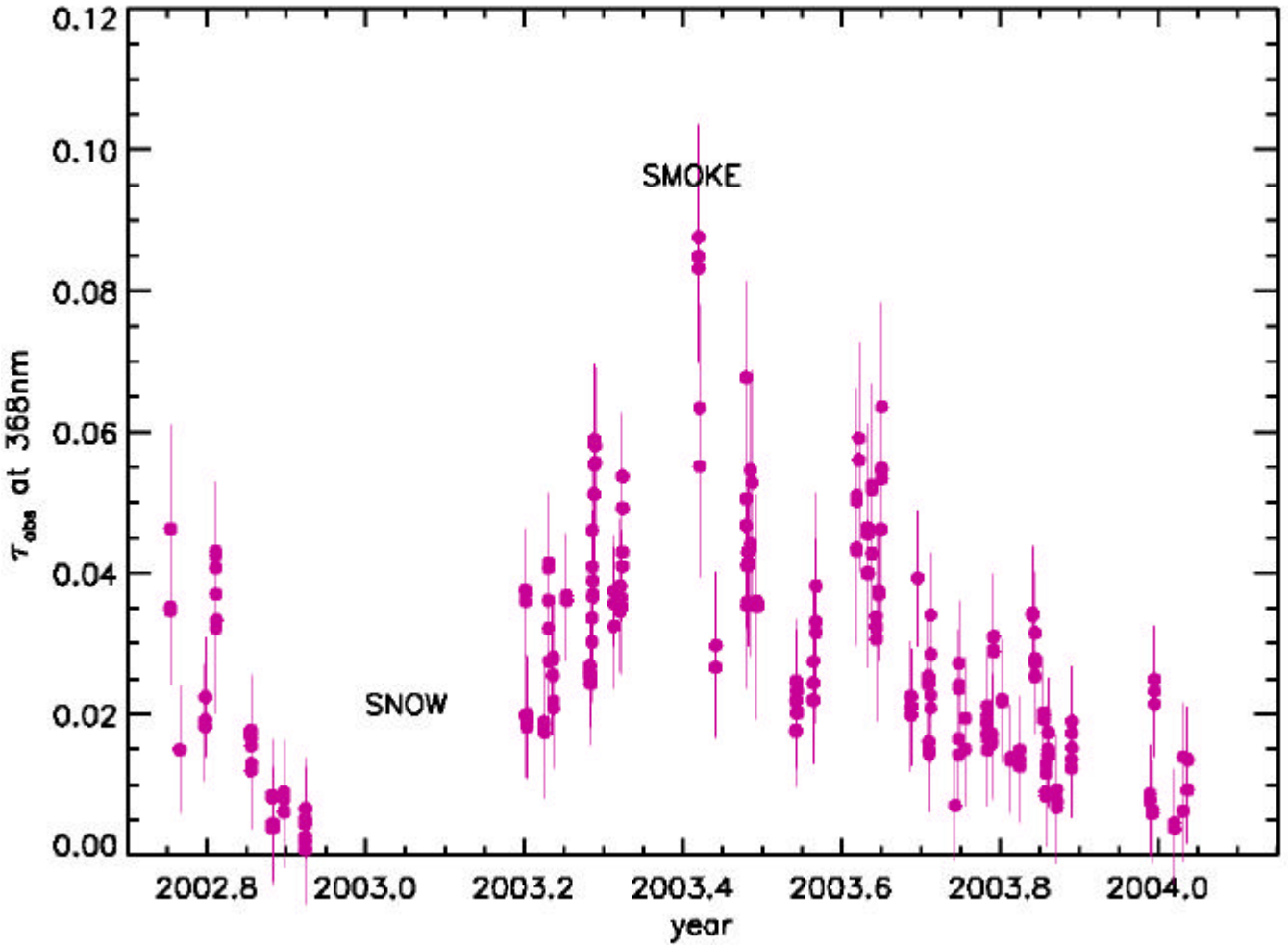


***Figure 5. Timeseries of aerosol absorption optical thickness $t_{abs}$ at 368nm, derived from 17 months UV-MFRSR operation at NASA GSFC site in Maryland, US. The data are for cloud-free and snow free conditions. Individual $t_{abs}$(368) values were averaged over period of time +/-30min.The error bars of $t_{abs}$(368) are interpolated by $t_{abs}$(368) and solar zenith angle from estimates given in Table 1.***

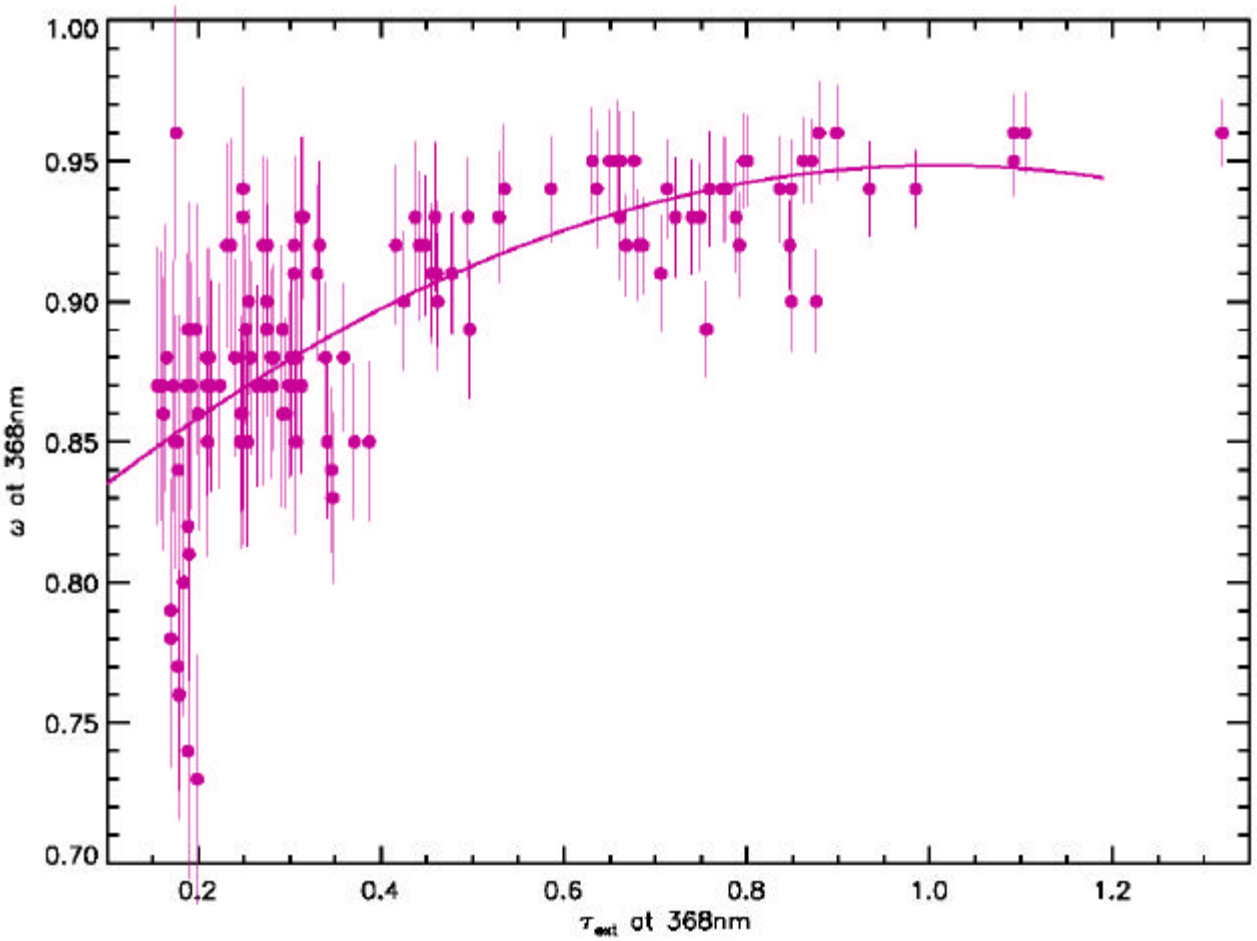


Figure 6. Hourly average retrieved values $< \omega_{368} >$ as function of measured extinction optical thickness, $\tau_{abs}$ at 368nm for 17 months UV-MFRSR operation at NASA GSFC site in Maryland, US. The error bars are interpolated from Table 1 and are the same as for individual retrievals. We do not reduce error bars despite 1 hour averaging of individual retrievals, because retrieval errors are not believed to be random. Only $< \omega_{368} >$ values with estimated uncertainties less than 0.05 are shown.